AD-A056 688 MASSACHUSETTS INST OF TECH CAMBRIDGE DEPT OF MATERIA--ETC F/G 7/3
ANALOGIES AMONG CHEMICAL PROPERTIES OF METAL SURFACES, ORGANOME--ETC(U)
JUL 78 K H JOHNSON N00014-75-C-0970

UNCLASSIFIED NL

1 OF 1
AD A056 688

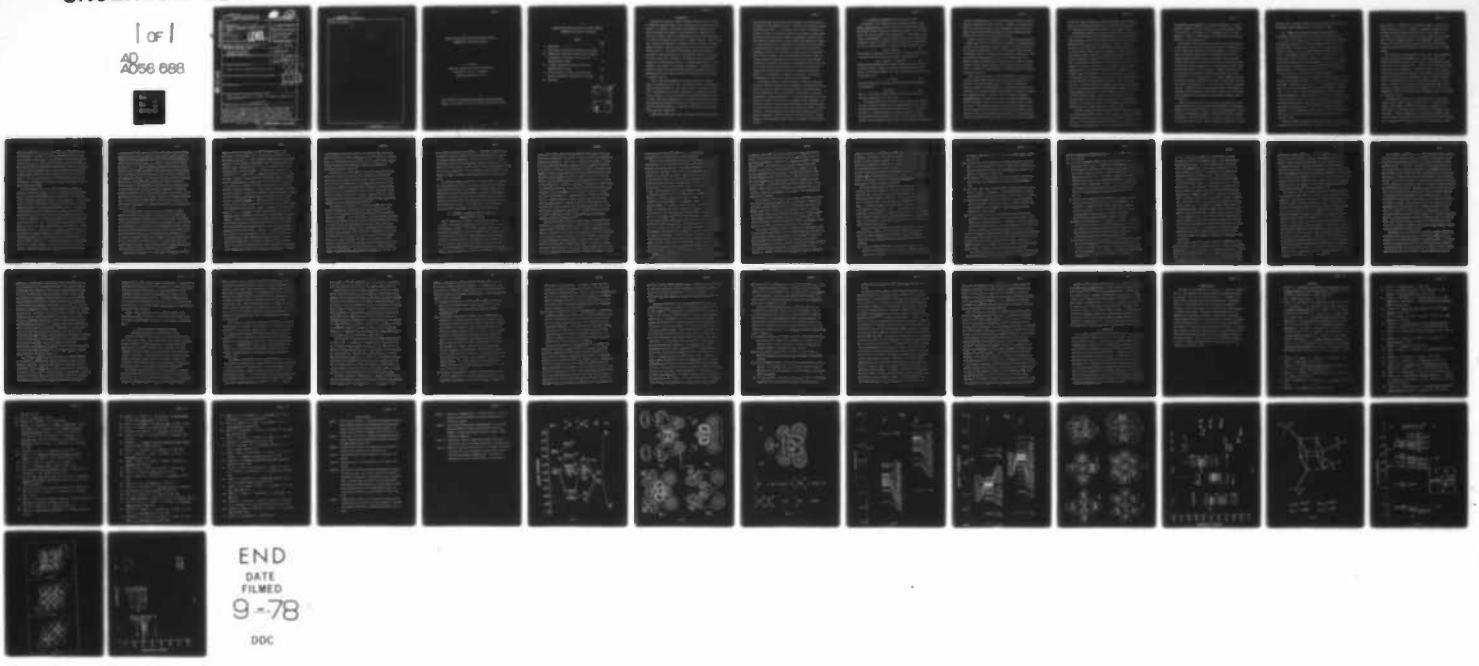

END
DATE FILMED
9-78
DDC

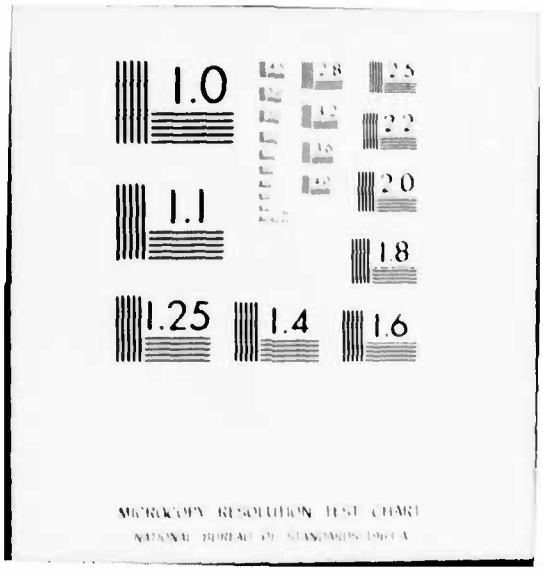
1.0
1.1
1.25
1.4
1.6
2.2
2.0
1.8
MICROCOPY RESOLUTION TEST CHART

UNCLASSIFIED
SECURITY CLASSIFICATION OF THIS PAGE (When Data Entered)

REPORT DOCUMENTATION PAGE

READ INSTRUCTIONS BEFORE COMPLETING FORM

1. REPORT NUMBER	2. GOVT ACCESSION NO. / 3. RECIPIENT'S CATALOG NUMBER
4. TITLE (and Subtitle): ANALOGIES AMONG CHEMICAL PROPERTIES OF METAL SURFACES, ORGANOMETALLIC MOLECULES, AND ENZYMES.	5. TYPE OF REPORT & PERIOD COVERED: Interim rept. / 6. PERFORMING ORG. REPORT NUMBER
7. AUTHOR(s): K. H. Johnson	8. CONTRACT OR GRANT NUMBER(s): N00014-75-C-0970
9. PERFORMING ORGANIZATION NAME AND ADDRESS: Department of Materials Science and Engineering, Massachusetts Institute of Technology, Cambridge, Massachusetts 02139	10. PROGRAM ELEMENT, PROJECT, TASK AREA & WORK UNIT NUMBERS: Task No. NR056-596
11. CONTROLLING OFFICE NAME AND ADDRESS: Office of Naval Research, Department of the Navy, Arlington, Virginia 22217	12. REPORT DATE: July 14, 1978 / 13. NUMBER OF PAGES
14. MONITORING AGENCY NAME & ADDRESS (if different from Controlling Office)	15. SECURITY CLASS. (of this report): Unclassified / 15a. DECLASSIFICATION/DOWNGRADING SCHEDULE

16. DISTRIBUTION STATEMENT (of this Report)

Approval for public release; distribution unlimited.

17. DISTRIBUTION STATEMENT (of the abstract entered in Block 20, if different from Report)

18. SUPPLEMENTARY NOTES

19. KEY WORDS (Continue on reverse side if necessary and identify by block number)

metal surfaces; organometallic molecules, spin-orbital electronegativity; catalytic activity.

20. ABSTRACT (Continue on reverse side if necessary and identify by block number)

In this paper, we point out a number of important similarities among the chemical (e.g., catalytic) properties of transition-metal surfaces, organometallic molecular complexes, and metalloenzymes, based on the electronic structures of such systems as calculated by the self-consistent-field X-alpha scattered-wave (SCF-Xα-SW) molecular-orbital method. The concept of 'spin-orbital electronegativity' is introduced as an approximate index of surface reactivity and catalytic activity as functions of composition, structure, and

DD FORM 1 JAN 73 1473 EDITION OF 1 NOV 65 IS OBSOLETE S/N 0102-014-6601

UNCLASSIFIED
SECURITY CLASSIFICATION OF THIS PAGE (When Data Entered)

409 463

molecular environment.

ANALOGIES AMONG CHEMICAL PROPERTIES OF METAL SURFACES, ORGANOMETALLIC MOLECULES, AND ENZYMES

K. H. Johnson

Department of Materials Science and Engineering

Massachusetts Institute of Technology

Cambridge, Massachusetts 02139

Paper presented at Third International Summer Institute in Surface Science. To be published in Critical Reviews in Solid State Sciences.

ANALOGIES AMONG CHEMICAL PROPERTIES OF METAL SURFACES, ORGANOMETALLIC MOLECULES, AND ENZYMES

Outline

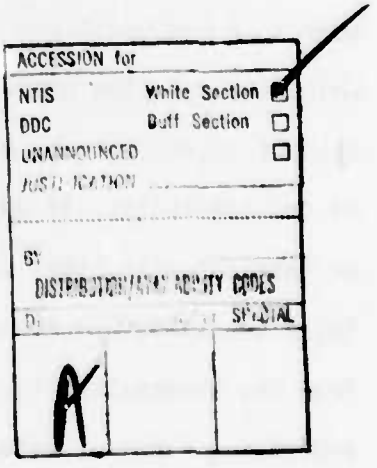

I. INTRODUCTION

The theorist who plans to study the chemical properties of surfaces from a fundamental electronic point of view is presented with a number of difficult problems. For example, if one focuses on heterogeneous catalysis by metal particles dispersed on a support,[1] should the electronic structure of the particles be viewed in terms of the band-structure theory of solid-state physics or in terms of the chemical-bond concept of inorganic chemistry? What are the most significant configurations of adsorbates which are precursors to heterogeneous reactivity? Does the supporting material affect chemisorption and catalytic activity? The theorist who calculates electronic structure is accustomed to having the positions and configurations of atoms in a molecule or solid as input to the calculation. Unfortunately, detailed structural information for heterogeneous catalysts is frequently unavailable and is just beginning to be a subject of experimental investigation. In contrast, the molecular structures of transition-metal coordination complexes involved in homogeneous catalysis[2] and enzymes involved in biocatalysis are often known to reasonable accuracy.

Given at least some knowledge of the catalyst molecular structure, a number of new questions can be asked. How mobile or labile are the adsorbates which are reaction precursors on the catalyst surface? Following the initial step of chemisorption, what reaction intermediates or decomposition products of the adsorbates, if any, are important? How do these intermediates convert or interact with other chemisorbed species to produce the reaction products? These questions are connected with the nature of the reaction kinetics and, from the theoretical viewpoint, are much more difficult to answer than those underlying simple chemisorption.

Keeping these limitations in mind, one may take a more optimistic outlook

and assess how theory, specifically quantum chemistry, can currently be used to promote the understanding of catalysis and other surface chemical properties at the electronic level. It is essential, first of all, to investigate the electronic structures of polyatomic aggregates and clusters of the types that constitute the active centers of commercial heterogeneous catalysts, along with theoretical studies of ideal crystal surfaces and chemisorption thereon. It is also important to try to understand the coordination chemical bonding of isolated transition-metal complexes of the type which are involved in homogeneous catalysis and the electronic structures of the biocatalytically active centers of enzymes. As will be emphasized in this paper, there are striking analogies between catalytically active sites on transition-metal surfaces and coordinatively unsaturated transition-metal complexes[2] (Section III), as well as analogies between the active centers of supported metal catalysts (Section IV) and the active centers of certain metalloenzymes (Section V). Such analogies are probably not fortuitous. They should be investigated and a common basis of understanding established.

In this paper we focus on a number of important similarities among the electronic structures of heterogeneous, homogeneous, and biological catalysts, using the results of recent self-consistent-field X-alpha scattered-wave (SCF-Xα-SW) molecular-orbital calculations.[3] Earlier phases of this work are described in previous publications.[4,5] One of the main objectives of such theoretical studies is the extraction of catalytic indices, dependent on the electronic structure of the catalyst, which would be an approximate gauge of the relative activity and selectivity of the catalyst with respect to certain reactants. The establishment of such indices could ultimately serve as a guide in the molecular design of catalysts for specific reactions. Recent progress in the development of such indices is the subject of the following section.

II. SPIN-ORBITAL ELECTRONEGATIVITY AND CATALYTIC ACTIVITY

An outgrowth of this theoretical work is the establishment of "spin-orbital electronegativity," defined by the SCF-Xα spin-orbital energies for representative surface clusters and coordination complexes, as a reactivity index of the type described in the preceding section. The concept of spin-orbital electronegativity is derived from the fact that the orbital energy eigenvalues in the SCF-Xα theory are rigorously equal to first derivatives of the total energy with respect to orbital occupation number,[3,6] i.e.,

$$\varepsilon_{i\mathrm{X}\alpha} = \partial\langle E_{\mathrm{X}\alpha}\rangle/\partial n_i \qquad (1)$$

These quantities should not be identified with the orbital energies defined in conventional Hartree-Fock theory,[6] namely, as the differences

$$\varepsilon_{i\mathrm{HF}} = \langle E_{\mathrm{HF}}(n_i=1)\rangle - \langle E_{\mathrm{HF}}(n_i=0)\rangle \qquad (2)$$

between single-determinant total energies calculated when the ith orbital is occupied and when it is empty (fixing the remaining occupied orbitals). The Xα orbital energies defined in Eq. (1) correspond closely to the orbital electronegativities

$$X_i = \partial E/\partial n_i \qquad (3)$$

defined by Hinze et al.[7] as a generalization of Mulliken's[8] definition of electronegativity

$$X_{\mathrm{M}} = \tfrac{1}{2}(I+A) \qquad (4)$$

where I is the ionization potential and A is the electron affinity of a chemically bonded atom in its valence state.

This generalization, its relationship to SCF-Xα theory, and ultimately its use as an index of reactivity can be understood better if one recalls that electronegativity, as originally defined by Pauling[9] is a measure of the power of a chemically bonded atom to attract electrons to itself. Pauling believed that electronegativity is a virtually constant atomic property, even for different valence states of the same element, and established

a scale of electronegativities for the elements based on the empirical bond energies of heteronuclear diatomic molecules. Despite the arbitrariness of this scale and the uncertainties in the thermochemical data on which it is based, a wide variety of chemical phenomena have been reasonably explained through the use of Pauling's electronegativity scale.

Pauling's concept of electronegativity as a fixed atomic characteristic is somewhat more restrictive than Mulliken's definition of electronegativity in terms of the valence-state ionization potential I and electron affinity A, since one does not expect that I and A or their average should be constant for different valence or oxidation states of a chemically bonded atom. Thus while Mulliken's electronegativity scale, in its simplest form, can be adjusted to agree reasonably well with Pauling's scale, element by element, Mulliken's concept is more satisfying from a theoretical point of view and allows, in principle, for the dependence of electronegativity on the chemical environment of an atom.

Since I and A are quantities related respectively to the removal of an electron from the highest occupied atomic orbital and the addition of an electron to the lowest unoccupied orbital, it might be expected that Mulliken's concept of electronegativity could be further generalized to all the orbitals of a chemically bonded atom and indeed to the molecular orbitals of an aggregate of atoms. Thus one is led to the concept of orbital electronegativity as a measure of the power of a chemically bonded atom or molecular aggregate to attract an electron to a particular atomic or molecular orbital. The mathematical definition of orbital electronegativity as the first derivative of the total energy with respect to occupation number, given in Eq. (3) in the form suggested by Hinze et al.,[7] is consistent with the above conceptual definition. Implicit in Eq. (3) are the two assumptions:

(a) that the occupation numbers n_i may have both integral and non-integral values; and (b) that once assumption (a) is made, then the total energy E is a continuous and differentiable function of the occupation numbers.

The occupation numbers n_i and statistical total energy $E_{X\alpha}$ defined in the Xα density-functional self-consistent-field theory fulfill both of the above conditions, so that one can uniquely identify the SCF-Xα electronic energy eigenvalues $\varepsilon_{iX\alpha}$ of an atom, molecule, or cluster, as given in expression (1), with the orbital electronegativities defined in Eq. (3). In the limit where the total energy is a quadratic (parabolic) function of the occupation number, the orbital electronegativity reduces exactly to Mulliken's definition of electronegativity given in Eq. (4).[7] This follows from a simple geometric theorem which relates the slope of the chord of a parabola to the slope of the parabola at its midpoint. The same type of argument applied to SCF-Xα orbitals leads to Slater's transition-state concept,[6] whereby one determines I or A for an atom, molecule, or cluster by subtracting or adding one-half a unit of valence orbital electronic charge and then calculating self-consistently the energy of the relaxed orbital. While these relaxed transition-state energies can be individually identified with the corresponding orbital ionization potentials or electron affinities, the unrelaxed ground-state SCF-Xα orbital energies $\varepsilon_{iX\alpha}$ define a set of orbital electronegativities. Thus the relative positions of the SCF-Xα electronic energy levels for a system of interacting or reacting atoms, molecules, or clusters are a measure of the orbital electronegativity and chemical-potential differences between the various reactants.

In those systems where magnetic spin polarization is important, one may use the spin-unrestricted version of the SCF-Xα method to calculate different orbitals for different spins, leading to spin-polarized energy levels $\varepsilon_{iX\alpha}{}^{\uparrow}$ and $\varepsilon_{iX\alpha}{}^{\downarrow}$.[3,6] If these spin-dependent orbital energies are identified with orbital electronegativities, then one is automatically led to the concept

of spin-orbital electronegativity as a measure of the power of an atom or molecular aggregate to attract an electron to a particular atomic or molecular spin orbital. For example, the spin dependence of orbital electronegativity is central to understanding the catalytic activity and surface reactivity of iron (see Section IV).

To understand the relationship between spin-orbital electronegativity, as represented by the SCF-Xα spin-orbital energy levels of representative surface clusters and reactants, and catalytic activity, it is helpful to recall the following concept originally introduced by Fukui.[10] For a concerted chemical reaction to occur with reasonable activation energy, electrons must be able to flow between the reactants from occupied orbitals into unoccupied orbitals with which they have net positive overlap, as the reactants move along the reaction coordinate. Overlap and electron flow will be ensured if the pertinent reactant orbitals have the following characteristics: (a) the same symmetry (i.e., orbital symmetry conservation as originally proposed by Woodward and Hoffmann[11]), and (b) equal or nearly equal orbital electronegativities. In the limit where electron flow between reactants is simply from the highest occupied molecular orbital (HOMO) to the lowest unoccupied molecular orbital (LUMO), condition (b) is equivalent to the requirement that the energy gap between HOMO and LUMO be as small as possible.[12]

Where direct electron flow between reactants is forbidden by orbital symmetry restrictions or unfavorable orbital electronegativity differences (implying a large activation energy), a surface can heterogeneously catalyze the reaction by providing a pathway for such electron flow, e.g., through chemisorption via spatially directed or hybridized d-orbitals in the case of a transition-metal surface. Similar arguments are applicable to isolated

transition-metal coordination complexes which homogeneously catalyze electron flow between reactants through bonding and exchange of ligands.

III. COORDINATIVELY UNSATURATED TRANSITION-METAL COMPLEXES AS ANALOGUES OF CATALYTICALLY ACTIVE SITES ON TRANSITION-METAL SURFACES

It is well known, for example, that certain "coordinatively unsaturated" transition-metal complexes in solution can homogeneously catalyze chemical reactions,[2,13] while it has long been suspected that low-coordination sites on transition-metal surfaces and supported transition-metal clusters are centers of heterogeneous catalytic activity.[14,15] In this section, it will be shown that the SCF-Xα electronic structure of such complexes, in conjunction with the concept of orbital electronegativity, is consistent with their reactivity and is suggestive of how low-coordination sites on transition-metal surfaces can act as centers of catalytic activity. The dissociation and reactivity of H_2 is considered as an illustrative example.

As a working model, we consider a Group-VIII transition-metal atom (M) dihedrally coordinated by ligands (L), yielding the coordinatively unsaturated L_2M complex illustrated at the top of Fig. 1. This model has the advantage that it can realistically represent transition-metal complexes of the type (e.g., M = Pt, Ir, Rh; L = Ph_3P = triphenylphosphine) which dissociatively bind and homogeneously catalyze reactions of H_2,[13] and it can simulate low-coordination sites (e.g., "corner atoms") of faceted transition-metal clusters or stepped transition-metal surfaces which dissociatively chemisorb and heterogeneously catalyze reactions of H_2.[14,15] In the latter systems, the ligand (L) is also a metal atom, either of the same species as the transition metal (M), or of a different species in the case of an alloy surface or bimetallic cluster.

Molecular-orbital calculations have been carried out for L_2M and L_2MH_2 complexes by the SCF-Xα-SW method as a function of metal species (M = Pt, Ir),

ligand species (L = phosphine, Pt), and molecular geometry. The resulting orbital energies for M = Pt, L = phosphine, and geometry characteristic of the platinum-phosphine complexes described in Ref. 13 are shown in Fig. 1. Also shown, for comparison, are the SCF-Xα orbital energies for the isolated metal, ligand, and hydrogen molecule at the free-molecule internuclear distance 0.74 Å (H_2) and internuclear distance 2.8 Å (H_2*) characteristic of the partially dissociated ("dihydride") configuration of H_2 in the L_2MH_2 complex.

The SCF-Xα orbital energy eigenvalues shown in Fig. 1 can be rigorously identified with orbital electronegativities which are a measure of the relative average electron donor-acceptor character of the individual orbitals, as described in the preceding section. Thus the fact that the isolated ligand energy level, which corresponds to a phosphine "lone-pair" orbital, nearly coincides with the d-orbital energy level of the isolated Pt atom (neglecting relativistic shifts) implies a predominantly covalent L-Pt(5d) interaction similar to that expected for a direct Pt(5d)-Pt(5d) interaction. In this respect, the effect of coordinatively unsaturated phosphine ligands on the electronic structure of a platinum atom is expected to be similar to that of embedding a Pt atom in a low-coordination Pt environment, such as that provided by a surface or cluster.

The ligand-metal interaction in the L_2M complex leads to the bonding orbital energies labeled L-M(d_{yz}) and L-M(d_{z2}) in Fig. 1, and to the anti-bonding orbital energies labeled M(d_{z2})-L*, M(d_{yz})-L*, and M(s)-L*, of which M(d_{yz})-L* is the highest occupied energy level in the ground state of the complex. A simple interpretation of the position of the latter energy level is that the strong ligand-field repulsion of the metal d-orbital pointed on the ligand directions (the d_{yz} orbital for the chosen coordinate system)

raises the energy level of this orbital, reduces the corresponding orbital electronegativity, and mixes in significant antibonding ligand character. The d_{z2} orbital is also subject to some antibonding ligand-field repulsion, whereas the d_{x2-y2}, d_{xz}, and d_{xy} orbitals remain essentially nonbonding. When platinum atoms are substituted for the phosphine ligands, the electronic structure reduces to the manifold of bonding, nonbonding, and antibonding d-orbital energy levels (the "d-band") characteristic of a small platinum cluster.[4] In this case, the $M(d_{yz})$-L* (L = M) antibonding orbital may be interpreted as the analogue of a localized "surface state" which is split off from the top of the d-band.

The most important result of the strong ligand-metal antibonding component is to bring the $M(d_{yz})$-L* orbital, the highest occupied orbital, closer in energy and electronegativity (as compared with the isolated Pt atom) to the empty antibonding σ_u orbital of the H_2 molecule. This facilitates overlap and electron flow between the $M(d_{yz})$-L* and σ_u orbitals, which are symmetry conserving,[11] thereby promoting dissociation of H_2. The partially dissociated molecule (H_2*), characterized by σ_g and σ_u orbital energies approaching the SCF-Xα 1s orbital energy of a free hydrogen atom (see Fig. 1), can bind or "chemisorb" in a dihydride configuration to the coordinatively unsaturated metal site. This is revealed by the L_2MH_2 molecular-orbital energies shown in Fig. 1 and the corresponding orbital wavefunction contour maps shown in Fig. 2. The $2b_2$ orbital, for example, results from overlap and electron flow between the $M(d_{yz})$-L* orbital and the H_2 σ_u orbital. The dihydride configuration is further stabilized by the "butterfly-like" $1a_1$ and $2a_1$ orbitals shown in Fig. 2, formed from the overlap of the equatorial parts of the L-$M(d_{z2})$ and $M(d_{z2})$-L* orbitals with the H(1s) (or H_2* σ_g) orbitals. Note that the $M(d_{z2})$ lobe pointed along the z-direction acts as

a repulsive barrier which helps to keep the H atoms apart. These dihydride bonding orbitals are offset somewhat by the $4a_1$ and $3a_1$ orbitals resulting respectively from the antibonding interaction of the L-M(d_{z^2}) and M($d_{x^2-y^2}$) orbitals with the H_2^* σ_g orbital, as is evident in the $4a_1$ orbital contour map shown in Fig. 2. There is negligible contribution of the M(s) orbital component in the binding of hydrogen to these platinum and iridium complexes. This is consistent with the finding, based on SCF-Xα cluster calculations[16] and photoemission studies,[17] that the metal d-orbitals are almost exclusively responsible for the chemisorption of hydrogen on second- and third-row transition metals such as palladium and platinum, whereas significant metal s,d-hybridization (with the s-orbital component dominant) is involved in hydrogen chemisorption on first-row transition metals such as nickel. Since the deuterium molecule (D_2) is orbitally identical to the hydrogen molecule (H_2), all the results described above for the dissociation of H_2 at a low-coordination transition-metal site apply equally well for the dissociation of D_2 at such a site.

The above-described electronic structure of the L_2MH_2 (or L_2MD_2) coordination complex leads to possible explanations of the observed homogeneous and heterogeneous catalytic reactivity of H_2 (or D_2). For example, the near cancellation of the contributions of the bonding ($1a_1$, $2a_1$) orbitals and antibonding ($3a_1$, $4a_1$) orbitals to metal-hydrogen bond strength, leaving the dissociative $2b_2$ bonding orbital dominant, explains the relatively weak, reversible binding of H_2 (or D_2) to such complexes and their ability to activate H_2-D_2 exchange.[13] Since such a complex is also a good model for H_2 (or D_2) dissociation at the corner atoms of a platinum surface step, the results suggest why atomic steps on platinum surfaces can be active sites for dissociating H_2 and D_2 and in activating H_2-D_2 exchange.[14,28]

The electronic structure of the L_2MH_2 complex also suggests a possible

reaction path for the hydrogenation of unsaturated hydrocarbons at low-coordination transition-metal sites. The $4a_1$ orbital, which defines the Fermi energy of the site, is closely matched in symmetry, energy, and electronegativity to the π orbitals of hydrocarbons such as acetylene (C_2H_2) and ethylene (C_2H_4). When the $4a_1$ orbital, which is an antibonding mixture of L-M(d_{z2}) and H_2^* σ_g orbital character, is only partially occupied (as is the case for M = Ir, Rh), it offers a pathway for electron flow from a C_2H_2 (or C_2H_4) π orbital to the dissociatively "chemisorbed" hydrogen. Electron flow directly between C_2H_2 (or C_2H_4) and H_2 in the gas phase via the filled π and σ_g orbitals is forbidden by the Pauli exclusion principle, whereas electron flow directly between the π orbital and empty σ_u orbital is forbidden by orbital symmetry.[11] Because the $4a_1$ orbital of L_2MH_2 is antibonding between the L_2M site and H_2, while bonding between H_2 and C_2H_2 (or C_2H_4), the net result of electron flow between a π orbital and the $4a_1$ orbital is the breaking of a C-C π bond, the formation of two new C-H bonds, and the expulsion of the hydrogenated species C_2H_4 (or C_2H_6), as suggested by the reaction path shown in Fig. 3. Also shown is a contour map for the $4a_1$ orbital of the $L_2MH_2C_2H_2$ reaction intermediate (the third step of the proposed reaction path) formed as a result of the interaction of acetylene with the L_2MH_2 complex. The incipient formation of C-H bonds via the overlap of the C-C π orbital with the antibonding metal-dihydride orbital and the resulting ethylene-like configuration are clearly visible in this map. It is important to note that the concerted reaction path indicated in Fig. 3 is not the conventional one for hydrogenation on ideal transition-metal surfaces, where it is usually assumed that chemisorption of acetylene or ethylene on one or two metal sites is the precursor to combining with hydrogen chemisorbed on neighboring sites. Nonconcerted reaction paths in which both reactants are coordinated

to the same metal site are also possible and indeed have been argued to be favored kinetically in certain homogeneous reactions.[18] Alternative reaction paths at low-coordination transition-metal sites are currently under investigation in conjunction with theoretical studies of the reactivity of $IrCl(CO)(Ph_3P)_2$ (Vaska's complex).[19]

In this section, we have attempted to show that a detailed theoretical study of the electronic structure of well characterized coordinatively unsaturated transition-metal complexes and their interactions with H_2 can not only lead to an understanding of their homogeneous reactivity but can also serve as a model for the dissociative chemisorption and heterogeneous reactivity of H_2 on low-coordination transition-metal surface sites, where definitive structural information is lacking. There are many other useful analogies which can be made between molecular transition-metal coordination complexes and surface-adsorbate interactions.[20,21]

In concluding this section, it is important to compare the present theoretical approach to surface reactivity, based on molecular-orbital indices, with other theoretical approaches to this problem and to chemical reactivity in general. In the applications of traditional methods of quantum chemistry (e.g., Hartree-Fock, Configuration-Interaction, Valence-Bond, etc.) to reaction kinetics and thermochemistry, one usually focuses directly on the calculation of total energies, total-energy differences, and "potential surfaces" for the reactants. This is generally a computationally difficult and costly process to carry out over the various possible reaction paths, even for the simplest reactions. To appreciate the magnitude of this problem, one need only consider the recent status of the quantitative first-principles determination of the kinetics of one of the simplest gas-phase chemical reactions, namely, hydrogen-deuterium exchange, $H_2 + D \rightarrow HD + H$.[22]

This situation hardly makes one confident in the efficacy of quantum theory to "predict" the path or kinetics of surface-activated reactions on the basis of potential-surface computations. Even if one carries out total energy calculations for only a few representative molecular configurations, rather than for the entire potential surface, there is still the uncertainty associated with the direct subtraction of two total energies, which are usually large numbers, to obtain a relatively small energy difference of chemical significance.

The theoretical approach described in this paper, while not a substitute for ab initio potential-surface calculations, circumvents many of the difficulties associated with the latter approach. By placing emphasis on the determination of molecular-orbital indices of reactivity, rather than total energies, for realistic transition-metal coordination complexes and clusters simulating local bulk and surface configurations, one retains the molecular-orbital picture which chemists have traditionally used and makes contact with the band-structure concept of solid-state and surface physics.

IV. ELECTRONIC STRUCTURE AND CATALYTIC ACTIVITY OF TRANSITION-METAL CLUSTERS

There is much current interest in the electronic structures of small transition- and noble-metal aggregates which constitute the active centers of heterogeneous catalysts.[1,15,23] Metal aggregates less than 10 Å in size, referred to as "clusters" in order to distinguish them from larger particles or crystallites,[24] are of special importance because their electronic structures, catalytic properties, and interactions with supporting environments can, in principle, deviate from those characteristic of the bulk metals.

In recent publications,[4,16] the electronic structures of small copper, nickel, palladium, and platinum clusters, as calculated by the self-consistent-

field X-alpha scattered-wave (SCF-Xα-SW) molecular-orbital method,[3] have been described and compared with the results of similar calculations by semiempirical molecular-orbital methods. One is at first struck by the systematic similarities, rather than the differences, between the SCF-Xα electronic structures of the clusters and those of the corresponding bulk metals. For example, the manifolds of orbital energy eigenvalues for 13-atom clusters having the cubo-octahedral nearest-neighbor coordination characteristic of the fcc lattice exhibit all the principal features of the bulk band structures, e.g., overlap of the "d band" by the "s,p band," a sharp peak in the density of states around the Fermi energy for the Ni_{13}, Pd_{13}, and Pt_{13} clusters, increasing band width through this series, and magnetic spin polarization in the case of Ni_{13}.[4] More recent SCF-Xα studies of 4- and 6-atom nickel, palladium, and platinum clusters, including relativistic effects, indicate that even these small clusters exhibit most of the qualitative features of the crystalline band structure and can be utilized as a basis for understanding the nature of the interaction of hydrogen with these metals.[16] These predictions have been confirmed by spectroscopic studies of small noble- and transition-metal clusters isolated in inert matrices.[25,26]

Concurrent with these theoretical studies, Messmer and Salahub[27] have carried out SCF-Xα-SW calculations for aluminum clusters (and oxygen chemisorption thereon) containing up to 43 atoms. The results indicate that 25 atoms are sufficient to yield the detailed structure and 92% of the band width of the electronic density of states of crystalline aluminum, as measured by X-ray and photoelectron emission spectra. Increasing the cluster size to 43 atoms yields 99% of the crystalline band width. The studies are perhaps the most definitive test of the "real-space" cluster representation of solids and surfaces made thus far, since aluminum is traditionally viewed as a highly

delocalized nearly-free-electron metal for which the conventional "k-space" representation of solid-state physics is most appropriate.

While a small transition-metal cluster does indeed exhibit most of the characteristics of the crystalline band-structure, the molecular boundary conditions and the fact that most of the atoms of the cluster are effectively coordinatively unsaturated "surface" atoms lead to some important additional features of the electronic structure.[4] These include the appearance of localized orbitals split off in energy from the top and bottom of the cluster d-orbital manifold, which can be interpreted as the cluster analogues of the "surface states" split off from the bulk d band for an extended crystalline surface. Also associated with the cluster boundary conditions is a buildup of electronic charge density in the cluster interior, compensated for by a depletion of electronic charge at the cluster periphery. Since a faceted polyhedral (e.g., cubo-octahedral or icosahedral) cluster is the simplest globular analogue of a "stepped" crystalline surface, the effective positive charge on the atoms at the cluster periphery is analogous to the positive charge observed at the catalytically active edge atoms of a stepped transition-metal (e.g., platinum) surface.[28] The resulting electric field gradient at the cluster boundary, coupled with a high density of d orbitals spatially directed away from the coordinatively unsaturated atoms at the cluster periphery (see Fig. 17 of Ref. 4), can promote interaction and overlap of these orbitals with symmetry-conserving orbitals of adsorbates, catalytic reactant molecules, and supporting environments. Thus the electronic structures of small transition-metal clusters not only mimic the band structures of the corresponding crystalline metals, but also have distinct features that may be key to understanding the active centers of heterogeneous catalysts and catalytically active sites (e.g., "steps") on otherwise ideal crystalline surfaces.

Although nickel, palladium, and platinum clusters of the type studied in Refs. 4 and 16 are a logical starting point in the fundamental investigation

of catalysts, other Group-VIII transition metals are of comparable catalytic versatility and invite theoretical consideration. Among these, iron is the most widely used commercial catalyst for the synthesis of ammonia (the Haber process),[29,30] is used commercially as a catalyst in the Fischer-Tropsch synthesis of high-molecular-weight paraffins,[31] and is generally one of the most surface-active transition metals. The electronic structures and related properties of iron clusters are also of intrinsic interest in the ways they compare with the band structure and physical properties of bulk crystalline iron. Of particular importance are the magnetic states of iron clusters, their relation to the ferromagnetism of crystalline iron, and the influence, if any, of such magnetism on the catalytic activity and surface reactivity of this metal.

In its biological states, iron is also a center of biocatalytic activity. For example, iron-porphyrin complexes are the active centers of hemoglobin, cytochrome, and other hemoproteins key to all respiration and metabolism,[32] whereas Fe_4S_8 clusters (see Fig. 8) are the active centers of ferredoxin, an iron-sulfur protein that is believed to be involved in nitrogen fixation (the biological analogue of ammonia synthesis).[33] The fact that an iron-sulfur cluster can be a center of biocatalytic activity is intriguing, since sulfur is well known to be a poison of commercial iron catalysts.

This section is devoted, in part, to a discussion of the magnetic states of iron clusters, especially as a basis for understanding the local bulk and surface magnetic properties of crystalline iron, including the transition from ferromagnetism to paramagnetism. Also discussed is the possible relationship between iron cluster electronic structure and catalytic activity, utilizing the concept of spin-orbital electronegativity described in Section II. Finally, in Section V the electronic structure of iron-sulfur

clusters in ferredoxin is described and compared with the electronic structure of elemental iron clusters, Apart from the biological significance of these studies, the results show the importance of Jahn-Teller distortions in small clusters, give insight as to how sulfur can promote the biocatalytic activity of iron despite the fact that sulfur is usually an iron catalyst poison, and provide a structurally well characterized molecular analogue of a metal-catalyst-support system including the effects of catalyst-support interactions. Extensive applications of the SCF-Xα-SW method to hemoglobin have recently been made by Case and are reported elsewhere.[34]

SCF-Xα-SW molecular-orbital calculations have been carried out for a variety of iron clusters ranging in size from 4 atoms to 15 atoms.[35] In this section we focus on the results for 9- and 15-atom clusters having the body-centered-cubic (bcc) geometry characteristic of the local atomic arrangement in bcc crystalline α-iron. The calculations were implemented in spin-unrestricted form, i.e., different orbitals for different spins, in precisely the same fashion as described for nickel clusters in Ref. 4. The resulting spin-orbital energy eigenvalues for the Fe_9 and Fe_{15} clusters are shown in Figs. 4 and 5, respectively, labeled according to the irreducible representation of the O_h symmetry group. An arrow points to the highest occupied spin orbital and defines the "Fermi energy" of each cluster.

From the qualitatively similar spin-polarized electronic structures of the Fe_9 and Fe_{15} clusters, one can extract the following characteristics which are directly comparable with the band structure of ferromagnetic crystalline α-iron calculated by Tawil and Callaway[36] using an SCF-Xα-LCAO technique:

(1) The cluster electronic structures can be characterized in terms of manifolds of predominantly d-like spin orbitals bracketed in energy by orbitals which have significant s,p character (as labeled in Fig. 7),

in analogy to the overlap of the d band by the s,p band in bulk crystalline iron.[36]

(2) The Fermi level of each cluster passes through the center of the "spin-down" (↓) d-orbital manifold in a fashion similar to the intersection of the Fermi level with the center of the "minority-spin" d band of ferromagnetic iron (see Fig. 2 of Ref. 36).

(3) The exchange splitting and widths of the cluster d bands, particularly those for Fe_{15}, are comparable with the values for bulk ferromagnetic iron.

(4) The cluster total density of states shows a pronounced two-peak structure, which is primarily a consequence of the exchange splitting, consistent with the density of states for ferromagnetic iron (see Fig. 5 of Ref. 36).

(5) Bonding and antibonding cluster spin orbitals of t_{2g} and e_g symmetry, such as those shown in Fig. 6, have a spatial character similar to the energy eigenstates of ferromagnetic iron near the bottom and top, respectively, of the d bands.

(6) The $7t_{2g}\uparrow$ and $6e_g\uparrow$ orbitals are the lowest unoccupied *majority-spin* eigenstates of the Fe_{15} cluster (see Fig. 5) and are analogous to the majority-spin crystal eigenstates of ferromagnetic iron lying immediately above the Fermi energy (see the band labeled $H'_{25}G_2N_3$ in Fig. 1 of Ref. 36).

SCF-Xα calculations have also been carried out for a bcc Fe_9 cluster in which the boundary conditions have been modified to simulate the "embedding" of the cluster in an extended crystalline environment.[35] Although the correspondence between the cluster and crystalline electronic structures is somewhat improved, e.g., through an effective increase in the cluster d-band width, the main conclusions given above are essentially unaltered.

The cluster results can be further utilized as a basis for understanding the transition between collective ferromagnetism (or "superparamagnetism"[37])

and local paramagnetism with decreasing particle size or increasing temperature. For example:

(1) The average paramagnetic magneton numbers per atom for the Fe_9 and Fe_{15} clusters are 2.9 and 2.5, respectively, approaching the 2.2 value for ferromagnetic crystalline α-iron, whereas SCF-Xα results for smaller iron clusters, such as Fe_8 and Fe_4, suggest increasing magnetic moment approaching the atomic limit. The increasing magneton number with decreasing iron cluster size is supported experimentally by Mössbauer studies of small iron aggregates isolated in inert matrices[38] and may be contrasted with the decreasing magneton number with decreasing cluster size observed theoretically and experimentally for nickel (see Ref. 4).

(2) The partial-wave decomposition of the Fe_9 and Fe_{15} cluster spin orbitals indicates that the contribution of the 4s-like components to spin polarization, although relatively small in magnitude, is opposite in direction (antiparallel to) that of the dominant 3d-like components, in good agreement with the analysis of magnetic form factors in polarized neutron scattering data for crystalline iron.[39]

(3) Somewhat more spin density in the Fe_9 and Fe_{15} clusters is concentrated in the e_g orbitals than in the t_{2g} orbitals (see Fig. 6), providing a local model for the concentration of spin density along the [100] direction (the direction of easy magnetization) in crystalline α-iron, as deduced from neutron-diffraction measurements.[39,40]

(4) Neutron-diffraction studies of crystalline iron at temperatures greater than the Curie temperature T_c[41-43] suggest that short-range ordering of spins in the form of "spin clusters" ($\sim$ 10 Å in size) persists well into the paramagnetic region, and that the paramagnetic magneton number is approximately 25% greater than the value for ferromagnetic iron

($T < T_c$). It is obvious therefore that the electronic structure of crystalline iron in the paramagnetic region is more appropriately represented statistically by a local spin-polarized cluster model, than by the extended $\vec{k}$-space band-structure description, since the cluster electronic structure is not dependent on the assumption of long-range crystalline ordering of spins. Utilizing the bcc Fe_{15} cluster as a prototype model for a "spin cluster," we see that the virtual majority-spin orbitals, $7t_{2g}\uparrow$ and $6e_g\uparrow$ (see Fig. 5), in the ground state ($T = 0°K$) are within a fraction of an electron volt of the Fermi energy, in analogy to the lowest unoccupied majority-spin eigenstates of ferromagnetic crystalline iron [see item (6) described above]. Thermally induced "spin-flip" electronic excitations from the Fermi level (which intersects the minority-spin manifold) to the $7t_{2g}\uparrow$ and $6e_g\uparrow$ orbitals for $T > T_c$ results in an effective 30% increase of cluster magnetic moment and magneton number, thereby providing a good model for the observed increase in magnetic moment of crystalline iron in the paramagnetic region. Such excitations only slightly alter the average exchange splitting and total density of states of the cluster, consistent with the apparent persistence of the local density of states for crystalline iron at $T > T_c$ (as measured, for example, by photoemission), an experimental observation which heretofore has been inexplicable within the framework of conventional ferromagnetic energy-band theory.

We can benefit from the large effective surfaces presented by the Fe_9 and Fe_{15} clusters to discuss the catalytic activity, selectivity, and general surface reactivity of iron aggregates, as has previously been done for nickel, palladium, and platinum in Refs. 4 and 16. Among the manifolds of densely spaced d-orbital eigenstates of these clusters are levels which correspond to antibonding spin orbitals primarily localized on and spatially oriented

away from the cluster periphery or "surface," especially in the general vicinity of the Fermi energy. The $2t_{1g}\downarrow$ orbital mapped in Fig. 6 is one example. Many of these spin orbitals have the proper spatial character for symmetry-conserving[11] overlap with the orbitals of certain reactant molecules and are likely to be present in abundance on the surfaces of catalytic iron aggregates and particles of more general morphology. This argument is clarified by a direct comparison in Fig. 7 of the Fe_{15} cluster spin-orbital energies with the SCF-Xα molecular-orbital energies of N_2, CO, and O_2, the molecules which are key reactants in iron-catalyzed ammonia synthesis[29,30] Fischer-Tropsch synthesis,[31] and surface oxidation.[44]

As described in Section II, the SCF-Xα spin-orbital energy eigenvalues of a molecule or cluster define on a one-to-one basis a manifold of electronegativities, each of which is a measure of the average electron donor and acceptor character of the corresponding spin orbital. Thus the relative positions of the orbital energies of the Fe_{15} cluster and reactant molecules, N_2, CO, and O_2, as shown in Fig. 7, are a measure of the differences in orbital electronegativity among these components. An effect of the large exchange splitting in the iron clusters is to raise the minority spin d orbitals to higher energies in comparison with the non-spin-polarized limit, effectively reducing the orbital-electronegativity difference and enhancing covalent overlap between the cluster HOMO (those symmetry-conserving minority-spin orbitals in the vicinity of the Fermi energy) and the LUMO of molecules such as N_2, CO, and O_2 (see Fig. 7). Because the latter molecular orbitals are antibonding, overlap and concomitant reduction in the activation energy for effective electron flow between the iron HOMO and reactant LUMO should promote dissociation of the reactant molecules, a precursor to their catalytic reactivity. Dissociation of N_2, CO, and O_2 does indeed occur on iron surfaces at room temperature and low coverage.[44-47]

Also included for comparison in Fig. 7 are the SCF-Xα-SW orbital energies of a Pt_{13} cluster previously shown to exhibit most of the characteristics of the bulk and surface electronic structures of crystalline platinum or small particles thereof.[4] In contrast to iron, there is no exchange splitting of the platinum cluster d orbitals, corresponding to the nonmagnetic state of bulk platinum, and the intrinsically larger electronegativity of the platinum atom results in a higher effective orbital electronegativity of the platinum cluster. The inclusion of relativistic corrections to the electronic structure of the latter cluster, as described in Ref. 16, increases its effective orbital electronegativity even further. Consequently, the d orbitals around the Fermi level of the platinum cluster, although high in density, are poorly matched in energy and orbital electronegativity to the LUMO of N_2 and CO. Thus a high density of states around the Fermi energy is not a sufficient condition for catalytic activity. These theoretical results are consistent with the experimental fact that platinum, which is an excellent catalyst for some reactions, is inactive in promoting N_2 and CO dissociation and is a poor catalyst for ammonia and Fischer-Tropsch syntheses.[15,31] The above conclusions about the relationship between the orbital electronegativities of transition-metal clusters and the conditions for molecular dissociation thereon are very similar to those for molecular dissociation on transition-metal surfaces arrived at empirically by Brodén et al.[46]

Dissociation of O_2, the rate-limiting precursor to oxygen chemisorption and surface oxidation, occurs rapidly at relatively low temperatures and pressures on iron surfaces,[44] suggesting low activation energy. On platinum surfaces this process seems to be less facile,[48] generally requiring more stringent conditions for activation, such as the presence of surface "steps" which play the role of active sites.[49] Like the processes of N_2 and CO

dissociation considered above, the relative activities of platinum and iron for O_2 dissociation can be rationalized in terms of the respective orbital electronegativities defined by the SCF-Xα orbital energy eigenvalues shown in Fig. 7. The Fermi level of the Fe_{15} cluster, as well as that of other spin-polarized iron aggregates including crystalline α-iron, lies somewhat above the energy of the partially occupied π_g orbital of O_2, implying that O_2 is effectively electronegative with respect to this metal. The resulting electrophilic addition of electrons to the antibonding π_g orbital will promote O_2 dissociation. In contrast, the Pt_{13} Fermi level lies below the π_g orbital, indicating that O_2 is formally nucleophilic with respect to this cluster. Therefore, under normal circumstances, electron transfer between O_2 and a platinum aggregate of "surface" is in a direction which should favor bonding rather than dissociation of this molecule. Nevertheless, a platinum site can be "activated" for O_2 dissociation by placing the former in a low-coordination environment in which a strong ligand-metal antibonding interaction raises the energy (lowers the electronegativity) of the Pt electron transfer from the metal to dioxygen. Such an environment is provided by a coordinatively unsaturated platinum complex of the type recently investigated via the SCF-Xα-SW method by Norman,[50] or by the "edge" atoms on a platinum surface step,[51] as described in Section III.

In an attempt to elucidate further the mechanism of ammonia synthesis on iron catalysts, Yang[35] has also constructed theoretical models for the effects of "promoters" (substances which, added to the catalyst, enhance its activity[29]), as well as models for the surface nitride which is formed upon dissociation of N_2 on iron.[47] The principal effect of the promoter is electron donation to iron, which reduces the electronegativity difference and activation energy for electron transfer between the metal HOMO and N_2 LUMO (as

compared with pure iron), thereby promoting N_2 dissociation. The dissociative chemisorption of nitrogen results in the formation of a surface nitride with an effective negative charge which, in a reducing atmosphere, should facilitate protonation of surface nitrogen atoms, the formation of N-H bonds, and ultimately ammonia synthesis. An analogous argument applied to the dissociative chemisorption of CO on iron leads one to conclude that the formation of an iron surface carbide should facilitate C-H bond formation and Fischer-Tropsch synthesis.

Details of these theoretical studies, theoretical models for N_2 dissociation and ammonia synthesis on ruthenium and osmium catalysts, and the nature of catalyst-support interactions are the subjects of forthcoming papers.

V. THE ACTIVE CENTERS OF IRON-SULFUR PROTEINS AS BIOLOGICAL ANALOGUES OF SUPPORTED METAL CLUSTERS

Iron-sulfur proteins[52] contain at least one iron atom coordinated by one or more sulfur ligands. These proteins participate in many biologically important reactions, including photosynthesis, nitrogen fixation, and hydroxylation of steroids.[53] Because of their involvement in so many fundamental biological processes, iron-sulfur proteins are obviously of interest to biochemists. They have also attracted the attention of many inorganic and physical chemists and physicists because of their novel structural and spectroscopic properties, and the opportunity they provide for the application of a wide range of experimental techniques.[54]

Although the typical molecular weight of these proteins is between 6,000 and 20,000, there are only one or two iron-sulfur units (each unit may have one, two, or four iron atoms) in the proteins that are responsible for most of the observed physical properties and biological activity.

These iron-sulfur units are called "active sites" and they may be considered as biological analogues of the active centers of industrial supported metal catalysts. Over the past few years, Holm et al. have successfully synthesized small-molecular-weight analogues of the iron-containing active sites, corresponding to the 1-Fe,[55] 2-Fe,[56] and 4-Fe/8-Fe[57] proteins, whose spectroscopic and magnetic properties and X-ray structures parallel closely those of the protein active sites. These analogues provide realistic models for theoretical studies and the SCF-Xα-SW method can readily be applied to them. Such studies for the 1-Fe and 2-Fe analogues have been carried out by Norman and coworkers,[58] and preliminary results for a 4-Fe analogue have been reported by Yang et al.[59]

In this section, the electronic structure of the 4-Fe protein analogue $[Fe_4S_4^*(SCH_3)_4]^{2-}$ is discussed. (S* is referred to as "inorganic" sulfur in biochemistry as distinct from "organic" sulfur S.) This is the simplest 4-iron-sulfur protein analogue that has been synthesized by Holm and coworkers,[60,61] and it is equivalent to the active site of the reduced high-potential iron protein (HP_{red}) and the active site of the oxidized ferredoxin (Fd_{ox}), i.e., $[Fe_4S_4^*(SCH_3)_4]^{2-} \equiv HP_{red} \equiv Fd_{ox}$. (The high-potential iron protein can be isolated from the photosynthetic bacterium "chromatium vinosum," and the ferredoxin can be obtained from bacterium "peptococcus aerogenes."[62])

A fundamental understanding of the 4-iron-sulfur proteins may be key to understanding the mechanism of nitrogen fixation, the biological equivalent of ammonia synthesis.[33] Nitrogenase, which is the enzyme complex capable of reducing dinitrogen to ammonia, consists of one iron protein and one molybdenum-iron protein. It is believed that the Mo-Fe protein functions to bind nitrogen, and the Fe protein or an external ferredoxin[63] (containing 4-Fe-S units) supplies low potential electrons to effect the reduction.

More recently, it has been reported[63] that the Mo-Fe protein also contains 4-Fe-S units which are very similar to those found in the HP proteins.

From the point of view of catalytic chemistry, it is useful to study these 4-iron-sulfur proteins and their analogues, not only because it may possibly lead to a better understanding of the interaction mechanism between nitrogen and the corresponding active centers in a commercial catalyst, but also because it provides reasonable models for catalyst-support interactions and the effects of sulfur "poisoning." The biocatalytically active iron cluster embedded in a cage formed by the neighboring sulfur atoms and the surrounding organic ligands (for the detailed structure, see Fig. 8) is somewhat analogous to the embedding of a catalytically active iron aggregate in a supporting refractory material, typically silica or alumina in the case of a commercial catalyst.[15] Ironically, sulfur is a strong poison for commercial iron catalysts,[64] and the different roles it play electronically in the protein and in the catalyst are of great interest.

The structure[60] of the 4-iron-sulfur protein analogue $[Fe_4S_4^*(SCH_3)_4]^{2-}$ is shown in Fig. 8. It consists of a simple cube with four Fe atoms and four "inorganic" S* atoms placed on alternate vertices. Along each of the diagonals containing the Fe atoms, there is one "organic" S atom terminated by a methyl group CH_3. The ideal overall point symmetry is T_d and the average interatomic distances are also shown in Fig. 8. However, detailed X-ray diffraction studies[60] indicate that the cube is slightly distorted into a lower D_{2d} symmetry, that the Fe-S-C angle is not exactly 180°, and that the symmetric interatomic distances are not exactly equal. All these deviations are treated as perturbations to the more symmetric model.

The orbital energies of $[Fe_4S_4^*(SCH_3)_4]^{2-}$, calculated by Yang[35] using the SCF-Xα-SW method and labeled according to the irreducible representations of the T_d point group, are displayed in Fig. 9. The highest occupied

orbital is indicated by an arrow, and the SCF-Xα energy levels for the free iron and sulfur atoms are shown for comparison. The energy scale is such that the top of the manifold of predominantly sulfur-like (S*-Fe) orbitals coincides in energy with the sulfur 3p atomic orbital. The following points emerge from this calculation:

(1) The number and character of occupied orbitals suggest that each Fe atom has the effective fractional valence state $Fe^{2.5+}$; discrete integral valence states are not spectroscopically detectable in $[Fe_4S_4^*(SCH_3)_4]^{2-}$.[65]

(2) The electronic inequivalence of S* and S atoms is emphasized by the findings that the charge localized in sulfur atomic regions averages 54.3 and 36.7% in the S*-Fe and Fe-S orbitals respectively, a behavior attributable to the influence of the electropositive metal in the structural fragments $S^*\text{-}Fe_3$ and Fe-S-C (cf. Fig. 8). Kramer et al.[66] measured the binding energies of the core electrons of reduced HP protein by X-ray photoelectron spectroscopy and found two sulfur 2p peaks at 162.9 eV and 161.5 eV, which they assigned to the S and S* atoms respectively. However, the SCF-Xα results suggest that a reversed assignment is more appropriate, since the local potential wells are deeper for the S* atoms than the S atoms because of stronger electropositive metal influence, and consequently greater core-electron binding energies. It is clear from Fig. 9 that, in general, the binding energies of the S* atoms are greater than those of the S atoms (e.g., the sulfur 3s levels).

(3) The band of levels between -0.35 and -0.15 Ry corresponds to orbitals ("Fe-Fe") predominantly Fe 3d-like in character and orbitals ("Fe-S") with almost equal amounts of Fe-3d and S-3p character. However, the

Fe-Fe levels are not purely metallic in nature, as compared with the orbitals of an isolated tetrahedral Fe_4 cluster (cf. Fig. 11) having the same Fe-Fe interatomic distance. The Fe-Fe orbitals in $[Fe_4S_4^*(SCH_3)_4]^{2-}$ have S 3p-like components ranging from only 3% S and 1% S* in the most metallic occupied bonding orbital (3e) to as much as 25% S and 12% S* in the least metallic unoccupied antibonding orbital (5e). Therefore, the Fe-S interactions are quite covalent.

(4) The highest occupied level ($10t_2$) in $[Fe_4S_4^*(SCH_3)_4]^{2-}$ is predominantly tetrametal antibonding in character, with S and S* contributions to the orbital charge amounting to 18 and 7% respectively. A contour map of the $10t_2$ orbital wavefunction is shown in Fig. 10(a), plotted in a $Fe_2S_2^*$ plane (cube face). This map reveals the 3d-like lobes centered on the Fe nuclei, polarized by in-plane and out-of-plane covalent interactions with S* and S 3p-like components, respectively. Also shown in Fig. 10(b) and 10(c) are the heavily tetrametal $8t_2$ and 3e orbitals which illustrate the net Fe-Fe bonding.

Optical absorption spectra for $[Fe_4S_4^*(SCH_3)_4]^{2-}$[57] are somewhat red-shifted but otherwise are similar to those of the proteins (HP_{red} and Fd_{ox}) and are dominated by intense features near 295 nm (4.20 eV) and 418 nm (2.97 eV), additional incompletely resolved bands at intermediate energies, and a low intensity shoulder at $\sim$ 650 nm (1.91 eV). According to the SCF-Xα calculation (Fig. 9), the intense peaks and fine structure between these peaks can be assigned as "charge-transfer" excitations from the band of predominantly sulfur-like levels lying between -0.48 and -0.58 Ry to the partially unoccupied tetrametal level $10t_2$. The top ($6t_2$) and bottom ($4a_1$) of the sulfur band are separated from the $10t_2$ level by the energies 2.98 and 4.32 eV, which are remarkably close to the energies 2.97

and 4.20 eV, of the principal absorption peaks. (Transition-state calculations[3,6] for these excitations have also been performed and the relaxation effects are small.) The low intensity shoulder at ∿ 1.91 eV is assigned to "d → d" electronic transitions between the occupied and unoccupied tetrametal ("Fe-Fe") levels.

The measured structure of the analogue $[Fe_4S_4^*(SCH_3)_4]^{2-}$ exhibits D_{2d} symmetry[60] and those of the biological counterparts HP_{red} and Fd_{ox} have D_{2d} or lower symmetry,[67,68] a property which is explicable in terms of the Jahn-Teller effect. From the calculated electronic structure of the $[Fe_4S_4^*(SCH_3)_4]^{2-}$ cluster (Fig. 9), the degeneracy of the partially occupied $10t_2$ orbital suggests the likelihood of a Jahn-Teller distortion from the perfectly cubic (T_d) geometry to one of lower symmetry. SCF-Xα-SW calculations for both the T_d and D_{2d} structures indicate a lower total energy for the distorted cube and a splitting of the $10t_2$ level into e and b_2 levels, as shown in Fig. 9(b). This splitting amounts of approximately 0.005 Ry (0.068 eV). The resulting "closed-shell" (zero-net-spin) electron configuration is consistent with the observed low-temperature diamagnetism of the analogue and HP_{red}.[69,70] The paramagnetism observed at higher temperatures[61,69,70] can be explained in the present model by the thermally induced excitation of electrons across the small $e \rightarrow b_2$ energy gap and the population of $b_2\uparrow$ states. Lastly, this model suggests that the oxidized species $[Fe_4S_4^*(SCH_3)_4]^{1-}$ and its biological counterpart HP_{ox} would have the $(10t_2)^3$ configuration (a half-filled shell) and hence, in the spin-unrestricted orbital description, would not be subject to Jahn-Teller distortions. Strong paramagnetism ($S = \frac{3}{2}$) should also be observed at low temperatures. No synthetic analogue of this oxidation state has been produced yet. However, it has been observed that in the biological state, the HP_{ox} site is marginally more symmetric than the HP_{red} site,[67]

and that the cluster volume contraction in the oxidation process $HP_{red} \rightarrow HP_{ox}$ is, as originally suggested,[67] partially accountable in terms of electron removal from an Fe-Fe antibonding orbital (the $10t_2$ orbital or its components in a lower symmetry). It has also been reported[63] that the 4-Fe-S site in the Mo-Fe protein isolated from "Azatobacter vinelandii" has a paramagnetic ground state corresponding to $S = \frac{3}{2}$.

In order to analyze the effects of the "supporting" sulfur-organic environment on the electronic structure of the 4-Fe aggregate, in Fig. 11 we compare the SCF-Xα energy eigenvalues of the predominantly tetrametal (Fe-Fe) orbitals of the $[Fe_4S_4^*(SCH_3)_4]^{2-}$ cluster (extracted from Fig. 9) with the spin-restricted orbital energies of a tetrahedral Fe_4 cluster in which the Fe-Fe internuclear distances have been constrained to the values in the 4-Fe-S cluster (cf. Fig. 8). The following conclusions can be derived from this comparison:

(1) Tetrametal bonding in the elemental Fe_4 cluster involves both d orbitals and s,p orbitals, in analogy to the overlap of the d band by the s,p "conduction" band in bulk iron, whereas in the protein analogue the tetrametal bonding is due entirely to the d orbitals.

(2) The high degeneracy around the Fermi level of the Fe_4 cluster is removed by "turning on" the sulfur-organic environment in the protein analogue.

(3) More antibonding tetrametal d orbitals are occupied relative to bonding orbitals in the Fe_4 cluster than in the protein analogue, indicating that the tetrairon d-orbital bonding is actually enhanced by the sulfur-organic environment.

(4) The total tetrametal d-band width in the protein analogue is significantly larger than that of the elemental Fe_4 cluster, consistent with the

stabilization of the bonding by the sulfur-organic environment implied in (3).

An even more dramatic comparison can be made between the tetrairon d-orbital manifold in the iron-sulfur protein analogue (Fig. 11) and the minority-spin (↓) d-orbital manifold in the Fe_{15} cluster analogue of a small iron particle (Fig. 7), in relation to the LUMO of the nitrogen molecule. This provides a common basis for understanding the biocatalytic mechanism of nitrogen fixation (reduction of dinitrogen to ammonia) by the enzyme nitrogenase[33] and the heterogeneous catalytic mechanism of ammonia synthesis (the Haber process)[29,30] by a commercial iron catalyst. As argued in Section IV, the local spin polarization of pure iron aggregates contributes to the reduction in activation energy (as compared with other metals) for the dissociation of N_2, the rate-limiting step of ammonia synthesis, by reducing the energy (and electronegativity) difference for electron flow between the catalyst HOMO and N_2 LUMO. In biological nitrogen fixation, it is speculated that the active center of the 4-Fe-S protein in nitrogenase reduces dinitrogen which is bound to an Mo-Fe protein.[33] In analogy to the suggested mechanism for N_2 dissociation by an iron catalyst (cf. Figs. 7 and 11), we see that this reduction can occur by electron transfer from the HOMO of the tetrairon d band of the 4-Fe-S cluster to the LUMO of N_2 (neglecting the perturbation of this LUMO by the Mo-Fe protein). Furthermore, the tetrairon HOMO is significantly closer in energy and electronegativity to the N_2 LUMO than in the case of Fe_{15} and larger iron aggregates, suggesting a lower activation energy for electron transfer. This seems to be consistent with the empirical fact that biological nitrogen fixation occurs efficiently at ordinary temperatures, whereas commercial ammonia synthesis is a high-temperature process. This theoretical model is further supported by the observation that the

active sites in nitrogenase are extremely sensitive to oxygen exposure,[53] suggesting the mechanism for O_2 bond cleavage and oxidation described for metallic iron in Section IV. Thus, while local spin polarization gives metallic iron an electron configuration which promotes the catalytic dissociation of N_2 and synthesis of ammonia, it is the supporting sulfur-organic environment which stabilizes the tetrairon cluster in an electron configuration highly favorable for dinitrogen reduction.

The final issue to be resolved is the apparent contradiction between the observation that sulfur effectively acts as a promoter of biocatalytic activity in iron-sulfur proteins, whereas it is well known to be a severe poison of iron catalysts in ammonia synthesis.[64] An examination of the electronic charge distribution in the $[Fe_4S_4^*(SCH_3)_4]^{2-}$ analogue, as calculated by the SCF-Xα method, suggests that the Fe(3d)-S(3p) and Fe(3d)-S*(3p) interactions in the corresponding protein are primarily covalent. This covalency is fairly apparent in the orbital contour maps shown in Fig. 10 and is confirmed experimentally by NMR contact shifts measured in the protein analogue.[61] Consequently, the tetrametal d orbitals are pushed closer in energy and electronegativity to the N_2 LUMO, as compared with those of an elemental iron cluster (cf. Figs. 11 and 7), because of the antibonding components of the iron-sulfur covalency. In contrast, the interaction of sulfur with metallic iron, as represented by the chemisorption of sulfur on an iron surface, is more ionic, withdrawing electrons from the metal to sulfur, thereby increasing the work function of the metal as well as the difference in energy and electronegativity between the iron HOMO and N_2 LUMO. Thus coordinative saturation of active iron surface sites by sulfur atoms, combined with the changes in effective iron orbital electronegativity, leads to a poisoning of iron catalysts for N_2 dissociation and ammonia synthesis.

Despite the wide-ranging similarities of the measured physical properties of analogues such as $[Fe_4S_4^*(SCH_3)_4]^{2-}$ to those of the active centers of the 4-Fe-S proteins,[57,60-62,65] the protein environment seems to be necessary for catalytic activity. Attempts to duplicate the full process of nitrogen fixation in the laboratory, using simpler synthetic analogues, have not yet been successful, although research in this area is important and continues.[33] It is not yet clear to what degree the extended organic environment of the active 4-Fe-S centers in the enzyme influences the local electronic structure and chemical properties of these sites, although SCF-Xα-SW studies[71] of the substitution of other simple organic ligands (including hydrogen) for the CH_3 moiety in $[Fe_4S_4^*(SCH_3)_4]^{2-}$ do not qualitatively alter the main features of the electronic structure shown in Fig. 9 and the conclusions based thereon.

VI. CONCLUSIONS

In this paper, we have attempted to elucidate a number of important analogies among the electronic structures of catalytically active sites on transition-metal surfaces, in isolated transition-metal coordination complexes, in supported metal catalysts, and in metalloenzymes, using the results of first-principles SCF-Xα molecular-orbital calculations in conjunction with the concept of spin-orbital electronegativity. Although an effort has been made to choose realistic illustrative examples for which there are comparable experimental data, some of the conclusions presented herein are speculative and hopefully will stimulate further experimental and theoretical work. It is hoped that such fundamental interdisciplinary studies will not only lead to a better understanding of the chemical properties of surfaces but will also serve ultimately as a guide for optimizing catalytic activity and selectivity through the systematic refinement of existing catalytic materials or through the molecular design of entirely new catalysts.

ACKNOWLEDGMENTS

The author is very grateful to his students, A. C. Balazs, D. Vvedensky, and C. Y. Yang, whose work has formed the basis for the examples presented in this paper. The author also wishes to thank Dr. R. P. Messmer of the General Electric Corporate Research and Development Center, Schenectady, New York, for many valuable discussions and continuing collaboration. Sponsorship of the various phases of this research by the following agencies is gratefully acknowledged: The National Science Foundation, Grant No. DMR74-15224, for sponsorship of research on metal clusters; the National Science Foundation through block funding provided to the Center for Materials Science and Engineering, M.I.T., for research on catalysis; the Office of Naval Research for supporting theoretical studies of reactivity at transition-metal interfaces; and grants from the donors of the Petroleum Research Fund, administered by the American Chemical Society, for theoretical research on iron-sulfur proteins. Finally, the author wishes to thank the organizers of the Third International Summer Institute in Surface Science for the opportunity to present this paper.

REFERENCES

1. Boudart, M., in Proceedings of the Robert A. Welch Foundation Conference on Chemical Research. XIV Solid State Chemistry, Milligan, W. O., Ed., The Robert A. Welch Foundation, Houston, Texas, 1970.
2. Ugo, R., Catal. Rev.-Sci. Eng., 11, 225, 1975.
3. Slater, J. B., and Johnson, K. H., Phys. Rev., B5, 844, 1972; Johnson, K. H., and Smith, F. C., Jr., Phys. Rev., B5, 831, 1972; Johnson, K. H., in Advances in Quantum Chemistry, Vol. 7, Löwdin, P.-O., Ed., Academic, New York, 1973, 143; Slater, J. C., and Johnson, K. H., Physics Today, 27, 34, 1974; Slater, J. C., The Self Consistent Field for Molecules and Solids, Vol. 4 of Quantum Theory of Molecules and Solids, McGraw-Hill, New York, 1974; Johnson, K. H., in Annual Review of Physical Chemistry, Vol. 26, Eyring, H., Christensen, C. J., and Johnston, H. S., Eds. Annual Reviews, Palo Alto, California, 1975, 39; Connolly, J. W. D., in Modern Theoretical Chemistry, Vol. 7, Segal, G. A., Ed., Plenum, New York, 1976; Messmer, R. P., in Modern Theoretical Chemistry, Vol. 8, Segal, G. A., Ed., Plenum, New York, 1977, 215; Rösch, N., in Electrons in Finite and Infinite Structures, Phariseau, P., and Scheire, L., Eds., NATO Advanced Study Institutes Series, Vol. 24, Plenum, New York, 1977, 1.
4. Messmer, R. P., Knudson, S. K., Johnson, K. H., Diamond, J. B., and Yang, C. Y., Phys. Rev., B13, 1396, 1976.
5. Johnson, K. H., in The New World of Quantum Chemistry, Pullman, B., and Parr, R., Eds., Reidel, Dordrecht-Holland, 1976, 317.
6. Slater, J. C., in Advances in Quantum Chemistry, Vol. 6, Löwdin, P.-O., Ed., Academic, New York, 1972, 1.
7. Hinze, J., Whitehead, M. A., and Jaffe, H. H., J. Am. Chem. Soc., 85, 148, 1963.
8. Mulliken, R. S., J. Chim. Phys., 46, 497, 675, 1949.

9. Pauling, L., J. Am. Chem. Soc., 54, 3570, 1932.

10. Fukui, K., Bull. Chem. Soc. Japan, 39, 498, 1966; Fukui, K., and Fujimoto, H., Bull. Chem. Soc. Japan, 39, 2116, 1966.

11. Hoffmann, R., and Woodward, R. B., Accounts Chem. Res., 1, 17, 1968; Woodward, R. B., and Hoffmann, R., The Conservation of Orbital Symmetry, Academic, New York, 1969.

12. Pearson, R. G., Theoret. Chim. Acta (Berlin) 16, 107, 1970; Accounts Chem. Res., 4, 152, 1971.

13. Ugo, R., La Monica, G., Cariati, F., Cenini, S., and Conti, F., Inorg. Chim. Acta, 4, 390, 1970.

14. Somorjai, G. A., in The Physical Basis for Heterogeneous Catalysis, Drauglis, E., and Jaffee, R. I., Eds., Plenum, New York, 1975, 395.

15. Anderson, J. R., The Structure of Metallic Catalysts, Academic, New York, 1975.

16. Messmer, R. P., Salahub, D. R., Johnson, K. H., and Yang, C. Y., Chem. Phys. Lett., in press.

17. Demuth, J. E., Surface Sci., 65, 369, 1977.

18. Cassar, L., Eaton, P. E., and Halpern, Jr., J. Am. Chem. Soc., 92, 3515, 1970.

19. Eberhardt, G. G., and Vaska, L., J. Catal., 8, 183, 1967.

20. Slater, J. C., and Johnson, K. H., Physics Today, 27, 34, 1974.

21. Messmer, R. P., in The Physical Basis for Heterogeneous Catalysis, Drauglis, E., and Jaffee, R. J., Eds., Plenum, New York, 1975, 261.

22. Koeppl, C. W., J. Chem. Phys., 59, 3427, 1973, and references therein.

23. Sinfelt, J. H., in Annual Review of Materials Science, Vol. 2, Huggins, R. A., Bube, R. H., and Roberts, R. W., Eds., Annual Reviews, Palo Alto, California, 1972, 641.

24. Johnson, K. H., and Hochstrasser, G., in The Physical Basis for Heterogeneous Catalysis, Drauglis, E., and Jaffee, R. J., Eds., Plenum,

New York, 1975, 373.

25. Ozin, G. A., Catal. Rev., in press.

26. Moskovits, M., and Hulse, J. E., to be published.

27. Messmer, R. P., and Salahub, D. R., Intern. J. Quantum Chem., 10S, 183, 1976; Messmer, R. P., and Salahub, D. R., in Computers in Chemical Research and Education, Ludéna, E. V., Sabelli, N., and Wahl, A. C., Eds., Plenum, New York, 1977; Messmer, R. P., and Salahub, D. R., Chem. Phys. Lett., 49, 59, 1977; Salahub, D. R., and Messmer, R. P., Phys. Rev. B, in press; Messmer, R. P., and Salahub, D. R., Phys. Rev. B, in press.

28. Christmann, K., and Ertl, G., Surface Sci., 60, 365, 1976.

29. Emmett, P. H., in The Physical Basis for Heterogeneous Catalysis, Drauglis, E., and Jaffee, R. I., Eds., Plenum, New York, 1975, 3.

30. Boudart, M., Topsøe, H., and Dumesic, J. A., ibid, 337.

31. Bond, G. C., Catalysis by Metals, Academic, New York, 1962.

32. See, for example, Hemes and Hemoproteins, Chance, B., Estabrook, R. W., and Yonetani, T., Eds., Academic, New York, 1966.

33. See, for example, Chem. and Eng. News, Sept. 24, 1973, 15; International Symposium on N_2 Fixation, Interdisciplinary Discussion, June 3-7, 1974, Pullman, Washington.

34. Case, D. A., Ph.D. Thesis, Department of Chemistry, Harvard University, June, 1977; Case, D. A., Huynh, B. H., and Karplus, M., J. Am. Chem. Soc., in press.

35. Yang, C. Y., Ph.D. Thesis, Department of Materials Science and Engineering, Massachusetts Institute of Technology, June, 1977.

36. Tawil, R. A., and Callaway, J., Phys. Rev. B7, 4242, 1973.

37. Abeles, B., in Applied Solid State Science, Vol. 6, Academic, New York, 1976, 90.

38. Montano, P. A., Barrett, P. H., and Shanfield, Z., Solid State Comm., 15, 1675, 1974; J. Chem. Phys., 64, 2896, 1976.

39. Shull, C. G., and Yamada, Y., J. Phys. Soc. Japan, 17S, BIII, 1, 1962.

40. Shull, C. G., and Mook, H. A., Phys. Rev. Lett., 16, 184, 1966.

41. Wilkinson, M. K., and Shull, C. G., Phys. Rev., 103, 516, 1956.

42. Gersch, H. A., Shull, C. G., and Wilkinson, M. K., Phys. Rev., 103, 103, 1956.

43. Averbach, B. L., in Magnetic Properties of Metals and Alloys, American Society for Metals, Chicago, 1959, 280.

44. Brucker, C. F., and Rhodin, T. N., Surface Sci., 57, 523, 1976.

45. Yu, K. Y., Spicer, W. E., Lindau, I., Pianetta, P., and Lin, S. F., Surface Sci., 57, 157, 1976.

46. Brodén, G., Rhodin, T. N., Brucker, C., Benbow, R., and Hurych, Z., Surface Sci., 59, 593, 1976.

47. Bozso, F., Ertl, G., Grunze, M., and Weiss, M., to be published.

48. Bonzel, H. P., and Ku, R., Surface Sci., 40, 85, 1973.

49. Lang, B., Joyner, R. W., and Somorjai, G. A., Surface Sci., 30, 454, 1972.

50. Norman, J. G., Mr., J. Am. Chem. Soc., 16, 1328, 1977.

51. Balazs, A. C., and Johnson, K. H., Chem. Phys. Lett., to be published.

52. Orme-Johnson, W. H., Ann. Rev. Biochem., 43, 814, 1974.

53. Hall, D. O., and Evans, M. C. W., Nature, 223, 1342, 1969.

54. See Iron-Sulfur Proteins, Lovenberg, W., Ed., Vol. 1-4, Academic, New York.

55. Lane, R. W., Ibers, J. A., Frankel, R. B., and Holm, R. H., Proc. Nat. Acad. Sci. USA, 72, 2868, 1975.

56. Mayerle, J. J., Denmark, S. E., Depamphilis, B. V., Ibers, J. A., and Holm, R. H., J. Am. Chem. Soc., 97, 1032, 1975.

57. Depamphilis, B. V., Averill, B. A., Herskovitz, T., Que, L., Jr., and Holm, R. H., J. Am. Chem. Soc., 96, 4168, 1975.

58. Norman, J. G., Jr., and Jackels, S. C., J. Am. Chem. Soc., 97, 3833, 1975; Norman, J. G., Jr., to be published.

59. Yang, C. Y., Johnson, K. H., Holm, R. H., and Norman, J. G., Jr., J. Am. Chem. Soc., 97, 6596, 1975.

60. Averill, B. A., Herskovitz, T., Holm, R. H., and Ibers, J. A., J. Chem. Soc., 95, 3523, 1973.

61. Holm, R. H., Phillips, W. D., Averill, B. A., Mayerle, J. J., and Herskovitz, T., J. Am. Chem. Soc., 96, 2109, 1974.

62. Holm, R. H., and Ibers, J. A., in Iron-Sulfur Proteins, Vol. IV, Chap. 7, Academic, New York, 1976.

63. Munck, E., Rhodes, H., Orme-Johnson, W. H., Davis, L. C., Brill, W. J., and Shah, V. K., Biochem. et Biophys. Acta, 400, 32, 1975.

64. Ashmore, P. G., in Catalysis and Inhibition of Chemical Reactions, Butterworth, London, 1963.

65. Holm, R. H., Averill, B. A., Herskovitz, T., Frankel, R. B., Gray, H. B., Siiman, O., and Grunthaner, F. J., J. Am. Chem. Soc. 96, 2644, 1974.

66. Kramer, L. N., and Klein, M. P., in Electron Spectroscopy, Shirley, D. A., Ed., North-Holland, Amsterdam, 1972, 733.

67. Carter, c. W., Jr., Kraut, J., Freer, S. T., and Alden, R. A., J. Bio. Chem., 249, 6339, 1974.

68. Adman, E. T., Sicker, L. C., and Jensen, L. H., J. Bio. Chem., 248, 3987, 1973.

69. Herskovitz, T., Averill, B. A., Holm, R. H., Ibers, J. A., Phillips, W. D., and Weiber, J. F., Proc. Nat. Acad. Sci. USA, 69, 2437, 1972.

70. Cerdonio, M., Wang, R.-H., Rawlings, J., and Gray, H. B., J. Am. Chem. Soc., 96, 6534, 1974.

71 Yang, C. Y., and Johnson, K. H., unpublished work.

FIGURE CAPTIONS

Figure 1. SCF-Xα orbital energies for coordinatively unsaturated transition-metal complexes representing low-coordination transition-metal sites and dissociative hydrogen chemisorption thereon. The highest occupied orbital is indicated by the "Fermi level" ϵ_F.

Figure 2. Contour maps of the principal bonding and antibonding molecular-orbital wavefunctions corresponding to the orbital energies of the L_2MH_2 complex shown in Fig. 1.

Figure 3. Possible reaction path for the hydrogenation of acetylene at a coordinatively unsaturated transition-metal site.

Figure 4. Spin-polarized SCF-Xα orbital energies of a 9-atom bcc iron cluster.

Figure 5. Spin-polarized SCF-Xα orbital energies of a 15-atom bcc iron cluster.

Figure 6. Contour maps of principal bonding and antibonding spin orbitals of bcc Fe_{15} cluster. Solid curves indicate positive parts of wavefunction; dashed curves indicate negative parts of wavefunction. e_g orbitals mapped in (100) plane containing central atom and second nearest neighbors; t_{2g} orbitals mapped in (110) plane containing central atom, nearest-neighbor atoms, and second nearest neighbors; t_{1g} orbital mapped in plane of cube face.

Figure 7. Comparison of the SCF-Xα orbital energies of the Fe_{15} and Pt_{13} clusters with those of the N_2, CO, and O_2 molecules. Also shown for comparison are the SCF-Xα atomic-orbital energies of N, C, and O.

Figure 8. Structure of $[Fe_4S_4^*(SCH_3)_4]^{2-}$, a synthetic analogue of the active center of oxidized ferredoxin and reduced high-potential four-iron-sulfur proteins.

Figure 9. (a) SCF-Xα orbital energies of $[Fe_4S_4^*(SCH_3)_4]^{2-}$ in T_d symmetry and (b) splitting of highest occupied orbital ($10t_2$) in D_{2d} symmetry. SCF-Xα atomic-orbital energies for Fe and S are also included for comparison.

Figure 10. Contour maps, plotted in $Fe_2S_2^*$ plane (cube face), for the (a) $10t_2$, (b) $8t_2$, and (c) 3e orbital wavefunctions of $[Fe_4S_4^*(SCH_3)_4]^{2-}$.

Figure 11. Comparison of SCF-Xα orbital energies for an elemental tetrahedral Fe_4 cluster with the corresponding tetrametal orbital energies for the protein analogue $[Fe_4S_4^*(SCH_3)_4]^{2-}$. Also shown for comparison are the SCF-Xα orbital energies of the N_2 molecule.

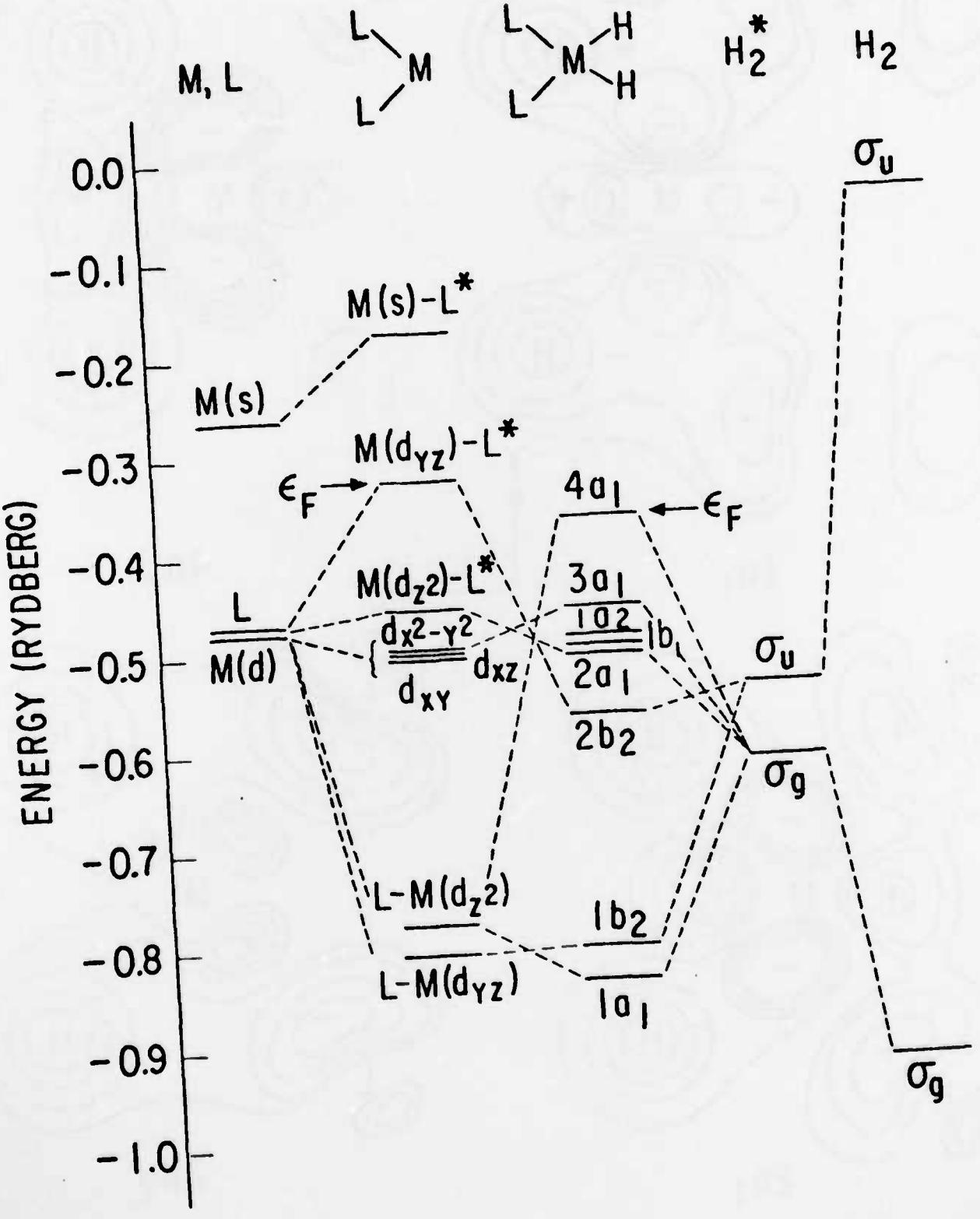
M, L
L
M
L
L
M
H
H
H_2^*
H_2
0.0
-0.1
-0.2
-0.3
-0.4
-0.5
-0.6
-0.7
-0.8
-0.9
-1.0
ENERGY (RYDBERG)
σ_u
M(s)-L*
M(s)
$M(d_{YZ})$-L*
ϵ_F
$4a_1$
ϵ_F
$M(d_{Z^2})$-L*
$3a_1$
L
M(d)
$d_{x^2-y^2}$
$1a_2$
$1b_1$
d_{xy}
d_{xz}
$2a_1$
σ_u
$2b_2$
σ_g
$L-M(d_{Z^2})$
$1b_2$
$L-M(d_{YZ})$
$1a_1$
σ_g

Figure 1.

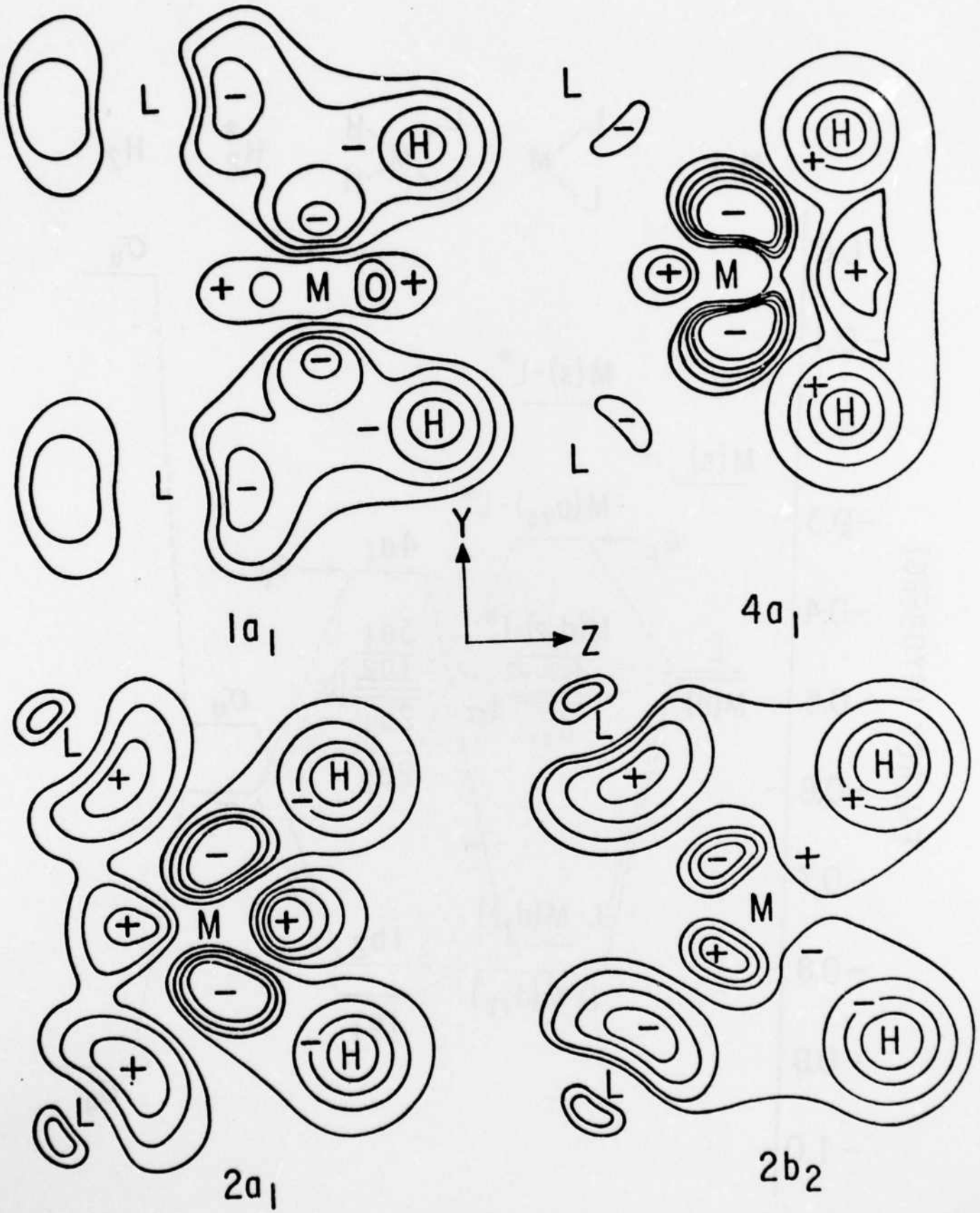

Figure 2.

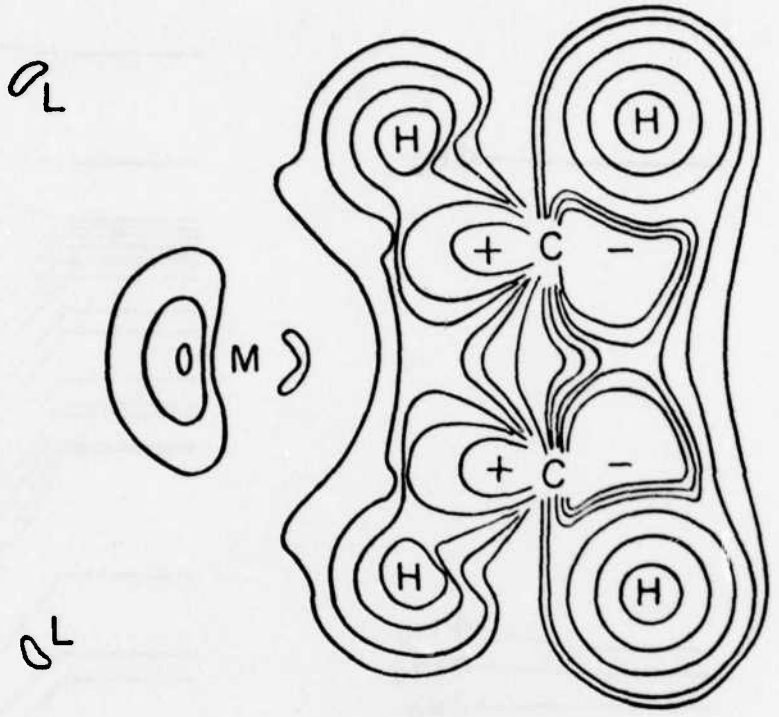

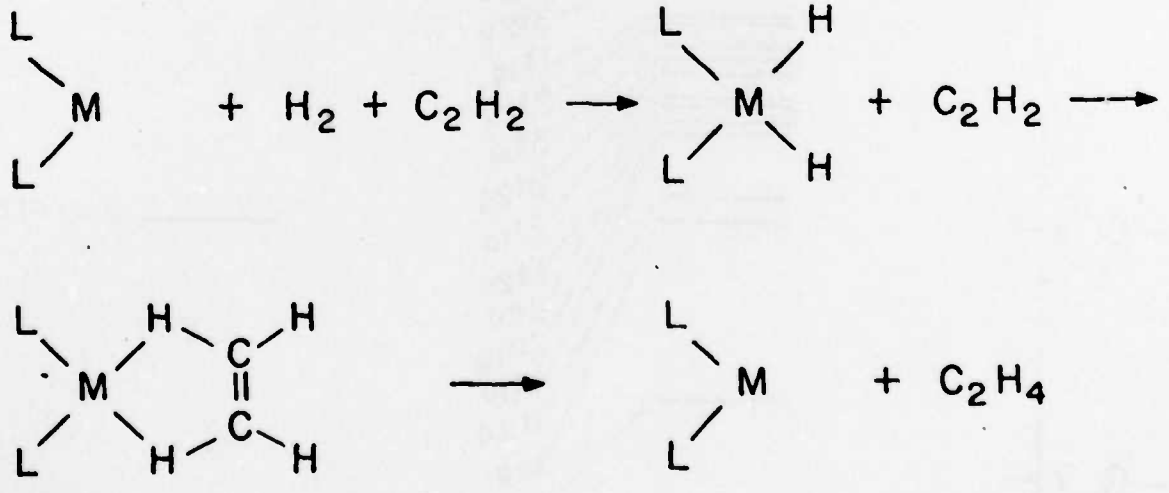

Figure 3.

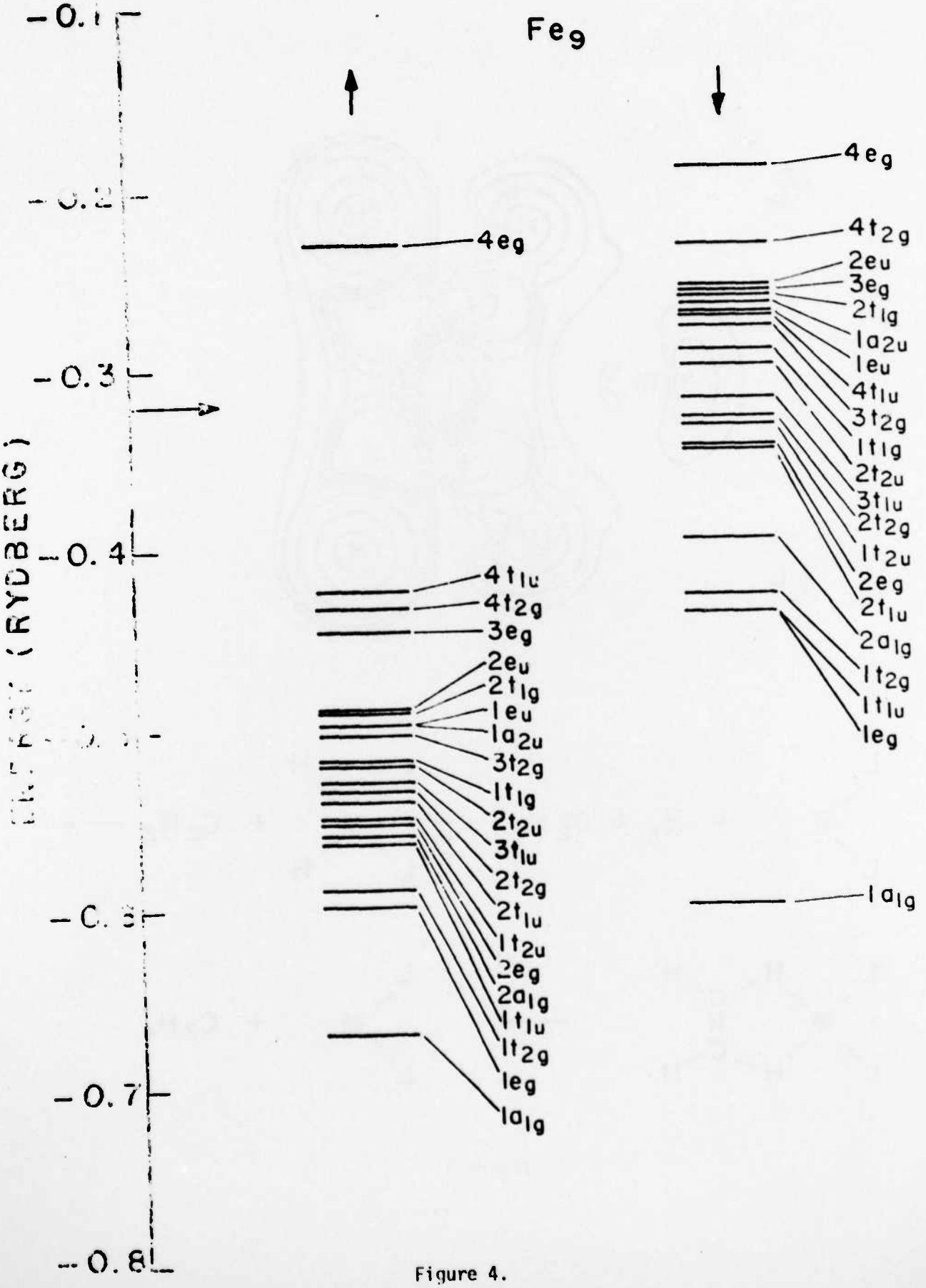
Fe9
-0.1
-0.2
-0.3
-0.4
-0.7
-0.8
(RYDBERG)
4eg
4t1u
4t2g
3eg
2eu
2t1g
1eu
1a2u
3t2g
1t1g
2t2u
3t1u
2t2g
1t2u
2eg
2a1g
1t1u
1t2g
1eg
1a1g
4eg
4t2g
2eu
3eg
2t1g
1a2u
1eu
4t1u
3t2g
1t1g
2t2u
3t1u
2t2g
1t2u
2eg
2t1u
2a1g
1t2g
1t1u
1eg
1a1g

Figure 4.

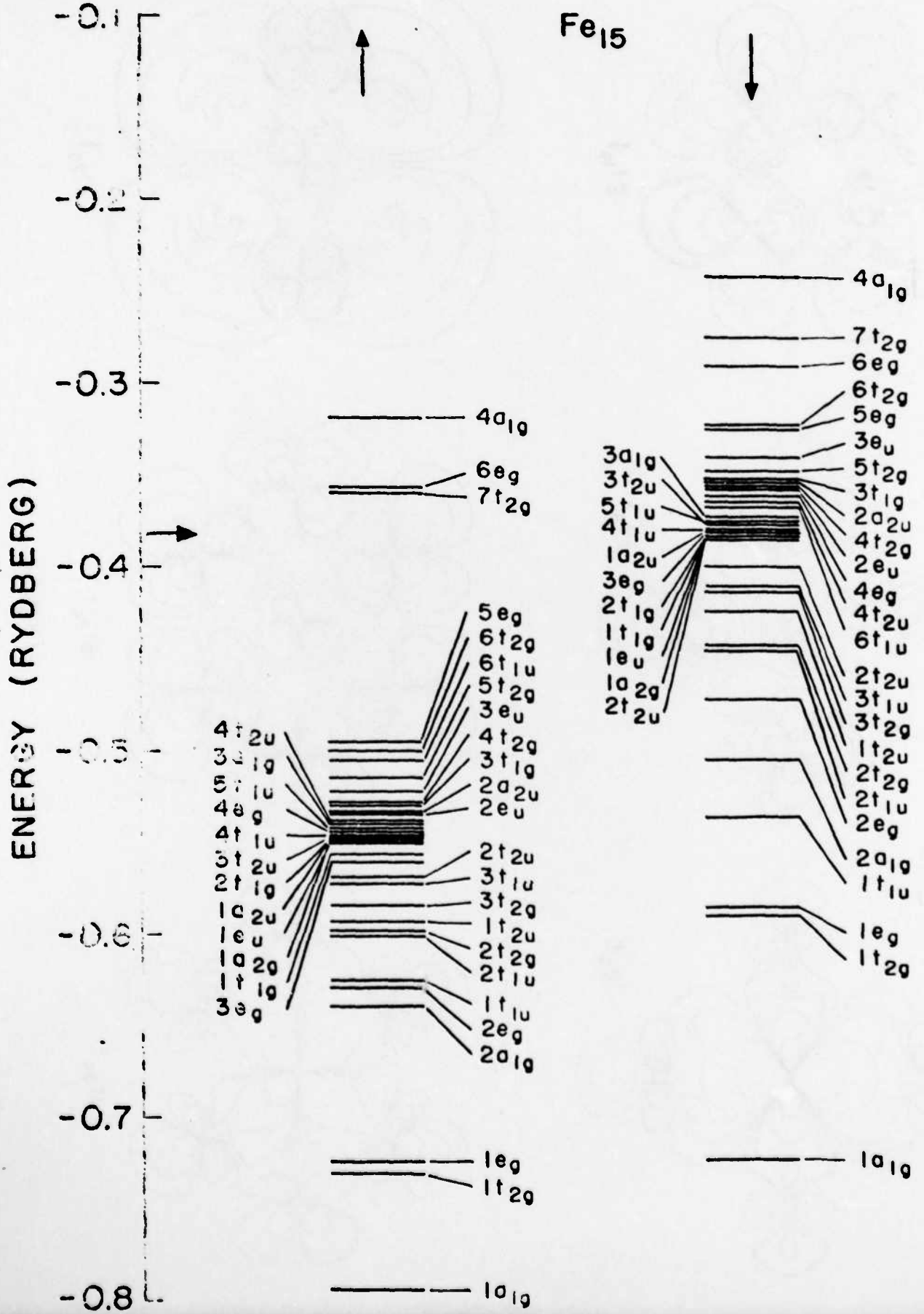
Fe15
ENERGY (RYDBERG)
-0.1
-0.2
-0.3
-0.4
-0.6
-0.7
-0.8
4a1g
7t2g
6eg
6t2g
5eg
3eu
3a1g
3t2u
5t1u
4t1u
1a2u
3eg
2t1g
1t1g
1eu
1a2g
2t2u
5eg
6t2g
6t1u
5t2g
3eu
4t2g
3t1g
2a2u
2eu
4t2u
3t2g
2t1g
1a2u
1eu
1a2g
1t1g
3eg
2t2u
3t1u
3t2g
1t2u
2t2g
2t1u
1t1u
2eg
2a1g
1eg
1t2g
1a1g

Figure 5.

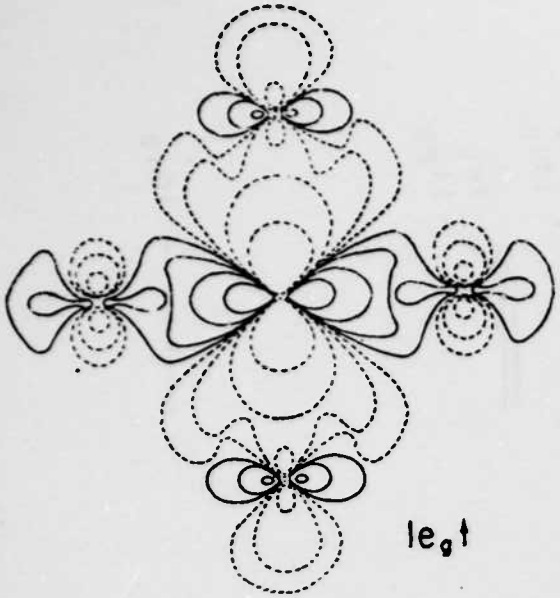
$1e_g\uparrow$

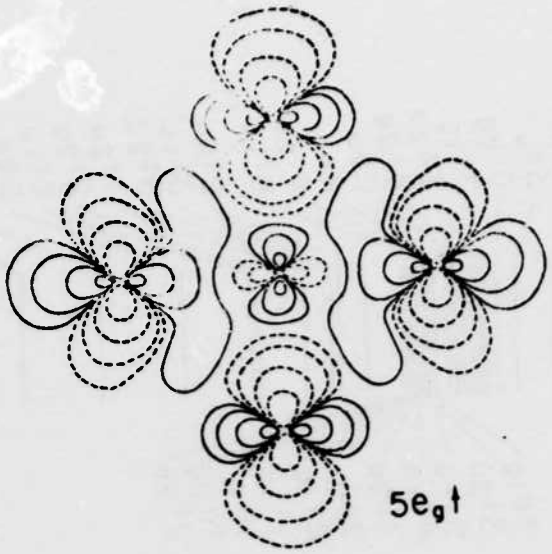
$5e_g\uparrow$

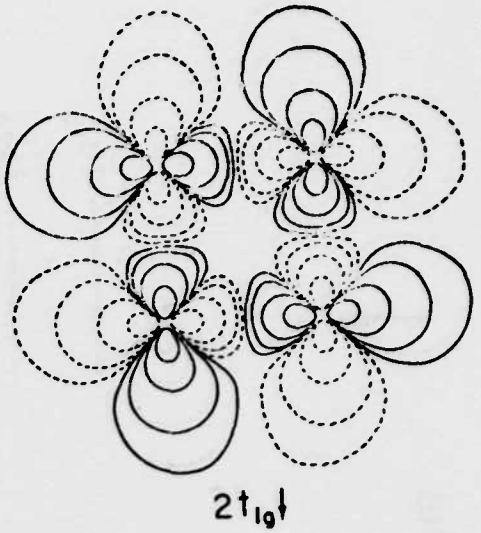
$2t_{1g}\uparrow$

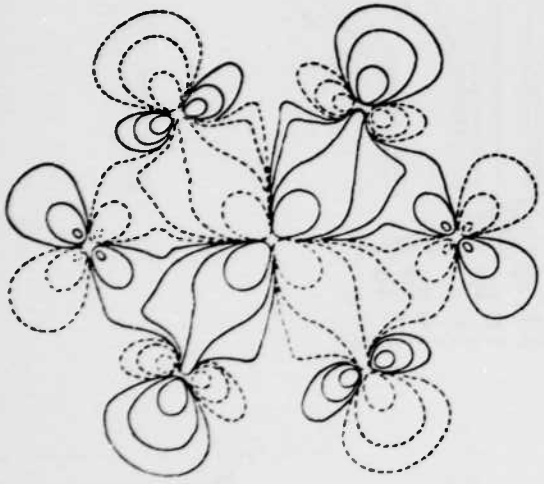
$1t_{2g}\uparrow$

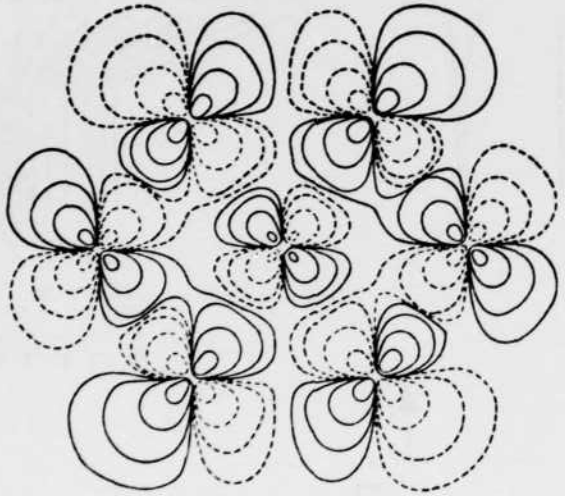
$6t_{2g}\uparrow$

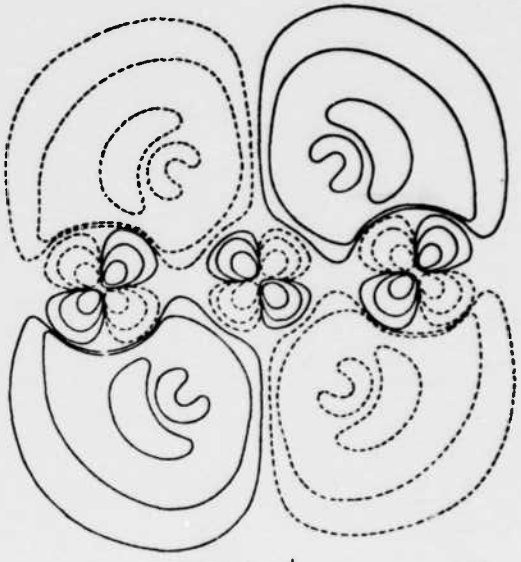
$7t_{2g}\uparrow$

Figure 6.

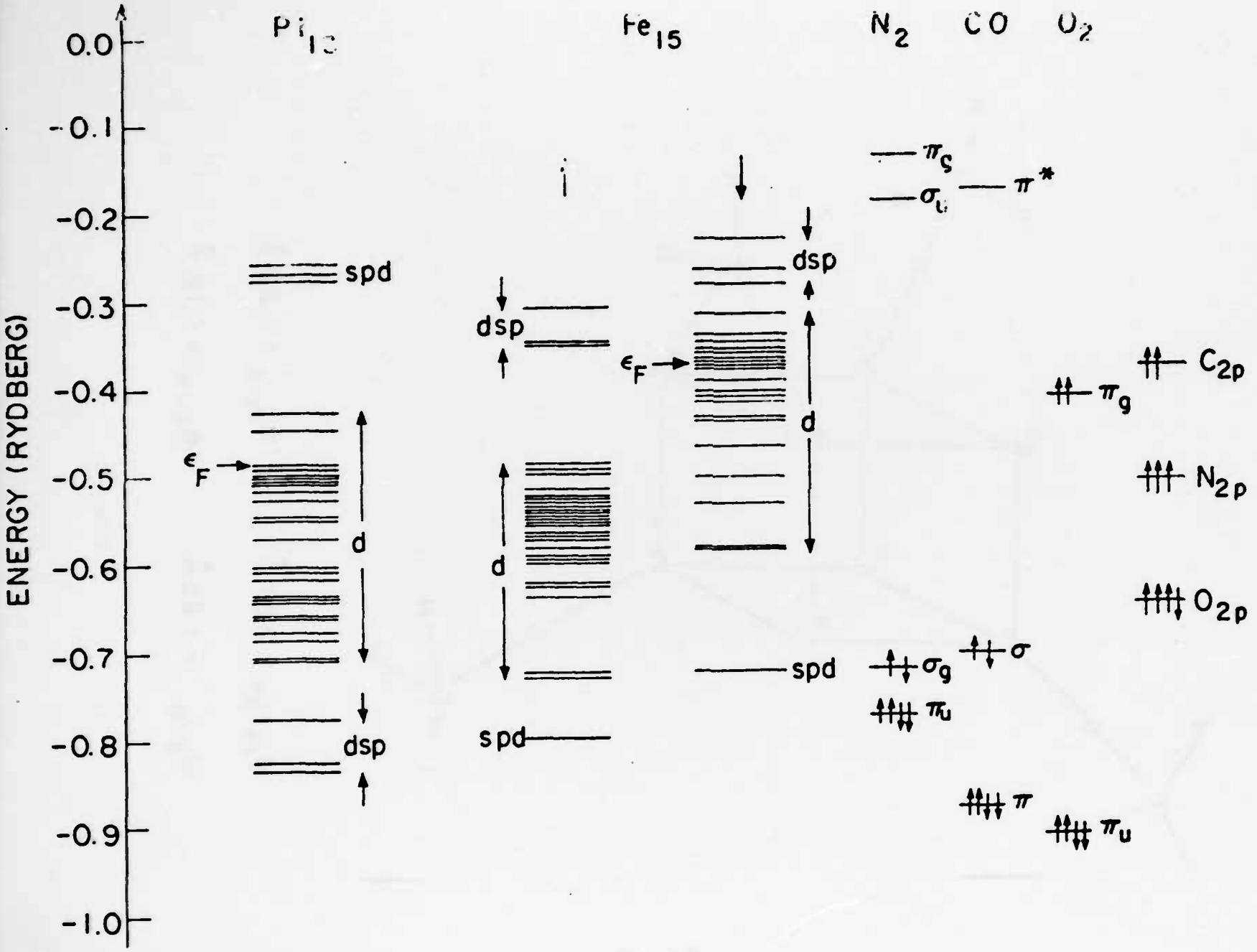
ENERGY (RYDBERG)
0.0
-0.1
-0.2
-0.3
-0.4
-0.5
-0.6
-0.7
-0.8
-0.9
-1.0
Pt13
Fe15
N2
CO
O2
spd
dsp
d
dsp
ϵ_F
ϵ_F
d
spd
dsp
d
spd
π_g
σ_u
π^*
C_{2p}
π_g
N_{2p}
O_{2p}
σ_g
σ
π_u
π
π_u

Figure 7.

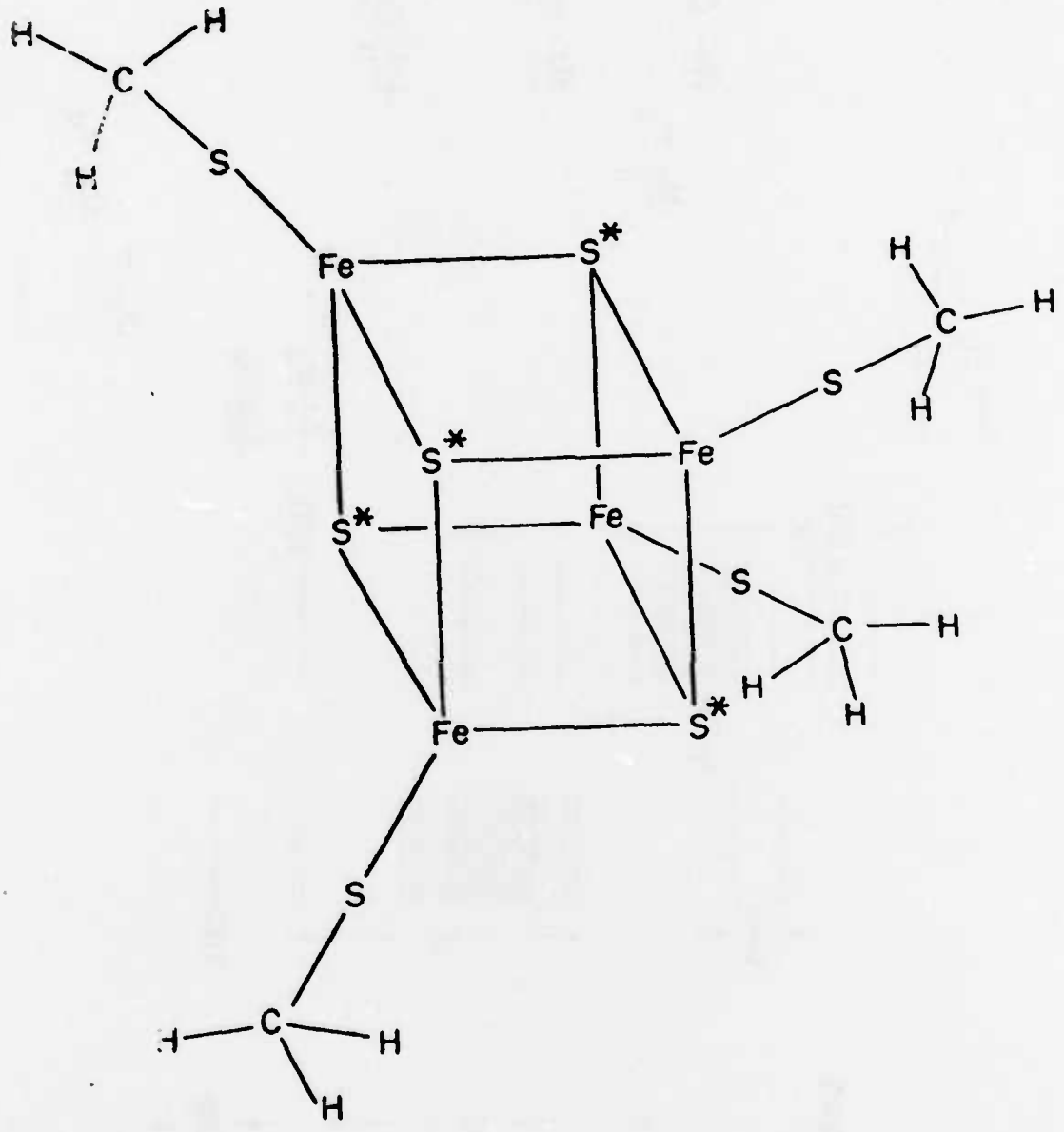

$d_{Fe-S^*} = 2.27$ Å $\qquad d_{Fe-S} = 2.25$ Å

$d_{S-C} = 1.83$ Å $\qquad d_{C-H} = 1.12$ Å

Figure 8.

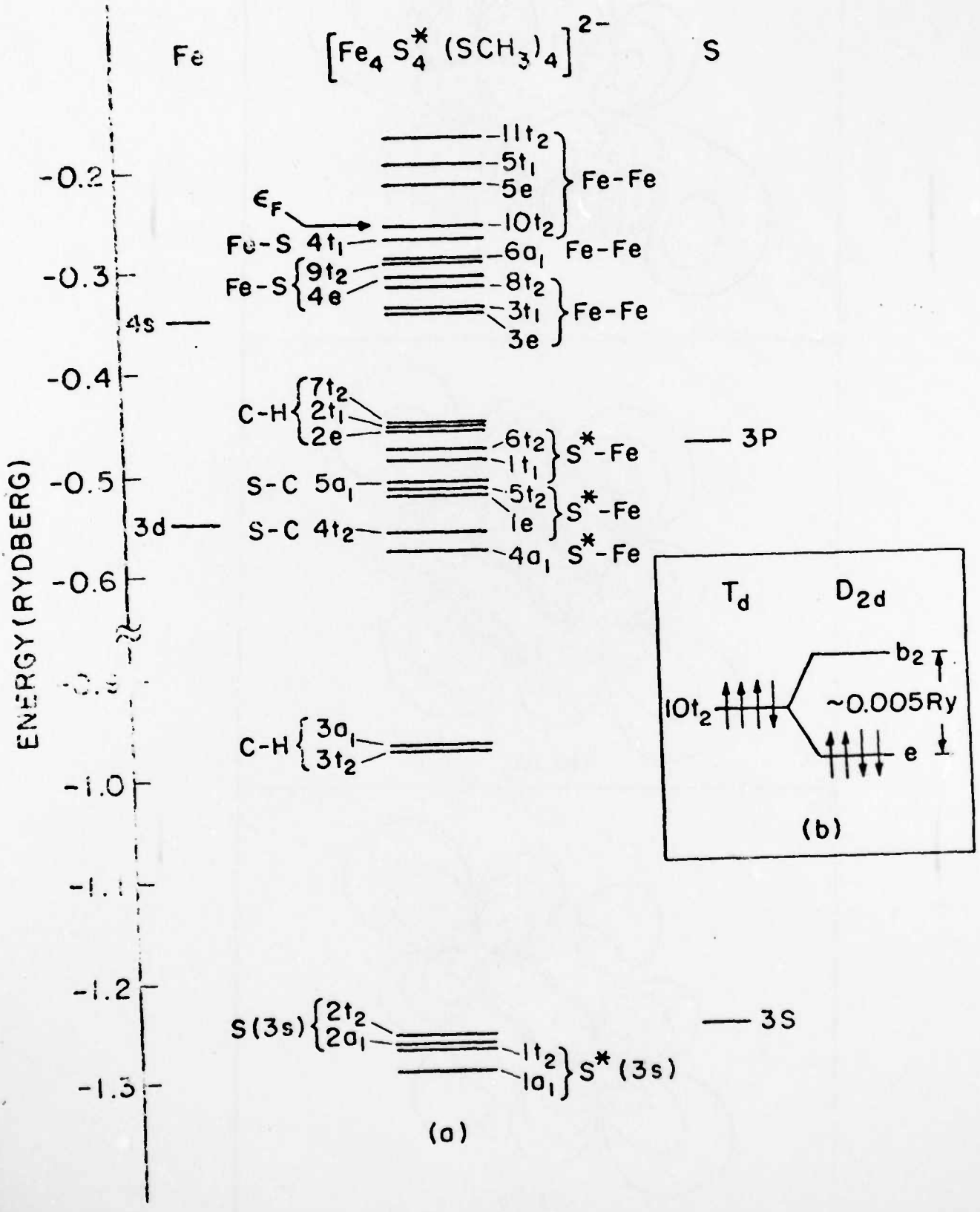
Fe
$[Fe_4 S_4^* (SCH_3)_4]^{2-}$
S
ENERGY (RYDBERG)
-0.2
-0.3
-0.4
-0.5
-0.6
-1.0
-1.1
-1.2
-1.3
4s
3d
ϵ_F
$11t_2$
$5t_1$
$5e$
$10t_2$
Fe-Fe
Fe-S $4t_1$
$6a_1$
Fe-Fe
Fe-S $9t_2$
$4e$
$8t_2$
$3t_1$
$3e$
Fe-Fe
C-H $7t_2$
$2t_1$
$2e$
$6t_2$
$1t_1$
S^*-Fe
3P
S-C $5a_1$
$5t_2$
$1e$
S^*-Fe
S-C $4t_2$
$4a_1$ S^*-Fe
C-H $3a_1$
$3t_2$
S(3s) $2t_2$
$2a_1$
$1t_2$
$1a_1$
S^*(3s)
3S
(a)
T_d
D_{2d}
b_2
$10t_2$
~0.005Ry
e
(b)

Figure 9.

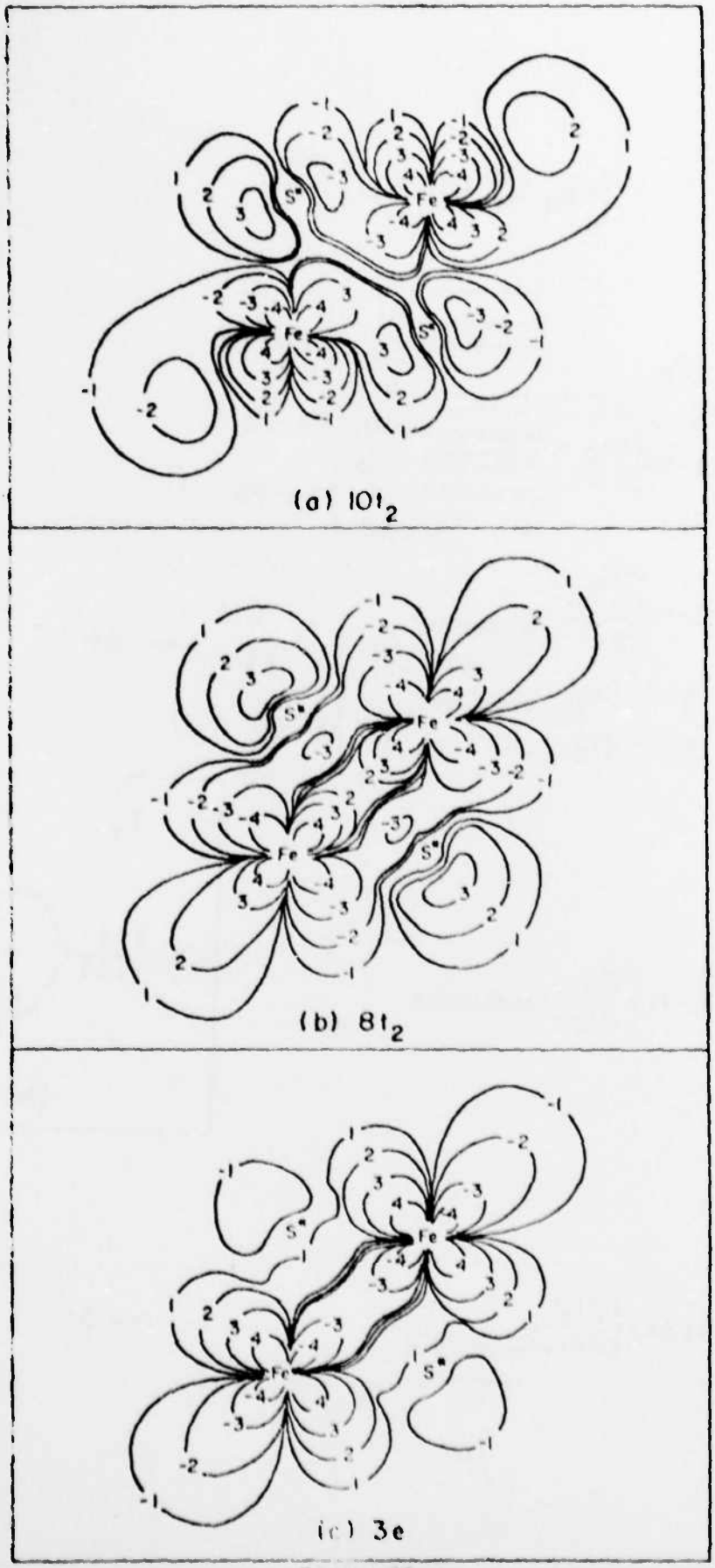

Figure 10.

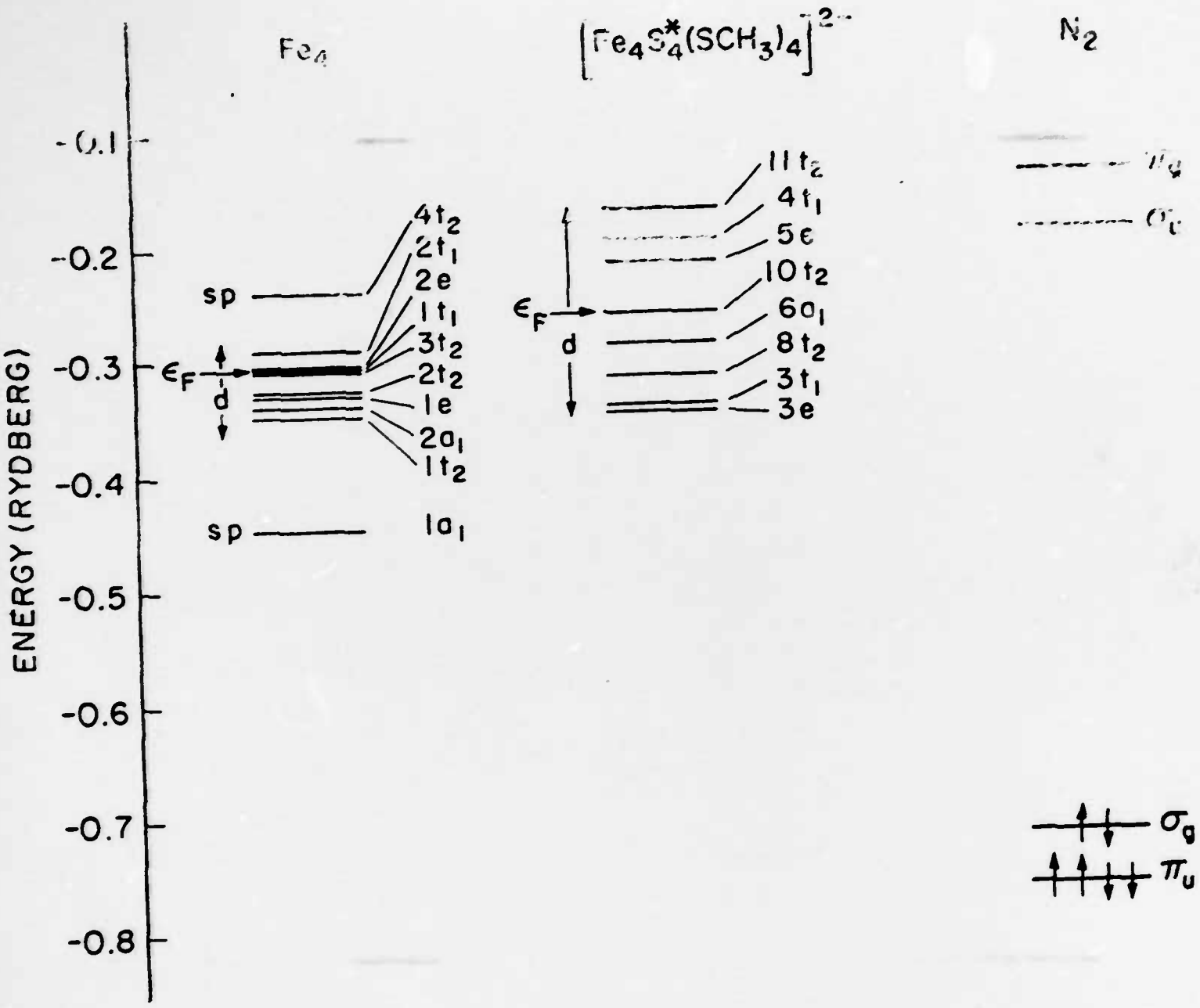
Fe4
[Fe4S4*(SCH3)4]2-
N2
ENERGY (RYDBERG)
-0.1
-0.2
-0.3
-0.4
-0.5
-0.6
-0.7
-0.8
sp
sp
d
d
εF
εF
4t2
2t1
2e
1t1
3t2
2t2
1e
2a1
1t2
1a1
11t2
4t1
5e
10t2
6a1
8t2
3t1
3e
σg
σu
πu
σg

Figure 11.